CHALMERS
UNIVERSITY OF TECHNOLOGY

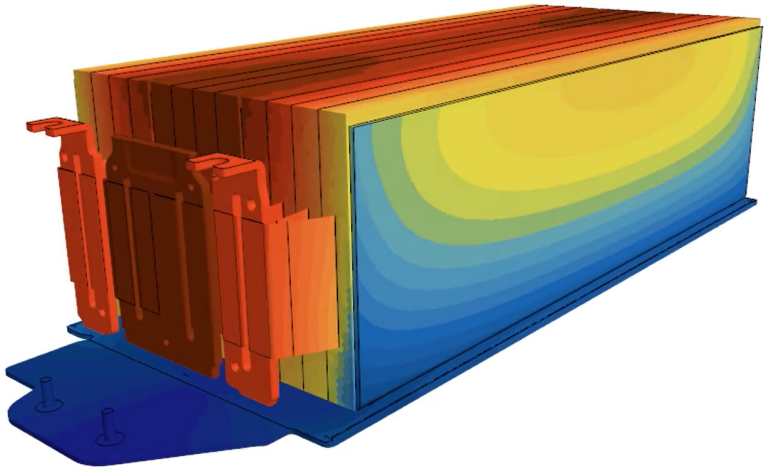

Time efficient simulations for advanced battery cooling concepts

enabling EV fast charging

Master's thesis in Mobility Engineering

SHANE SHAJU

DEPARTMENT OF MECHANICS AND MARITIME SCIENCES

CHALMERS UNIVERSITY OF TECHNOLOGY
Gothenburg, Sweden 2023
www.chalmers.se

Master's thesis 2023

Time Efficient Simulations for Advanced Battery Cooling Concepts

enabling EV fast charging

SHANE SHAJU

CHALMERS
UNIVERSITY OF TECHNOLOGY

Department of Mechanics and Maritime Sciences
Chalmers University of Technology
Gothenburg, Sweden 2023

Time Efficient Simulations for Advanced Battery Cooling Concepts
enabling EV fast charging
SHANE SHAJU

Supervisor: Anders Wedin and Jens Groot, Polestar
Examiner: Petter Dahlander, Department of Mechanics and Maritime Sciences

Master's Thesis 2023
Department of Mechanics and Maritime Sciences
Division of Division name
Name of research group (if applicable)
Chalmers University of Technology
SE-412 96 Gothenburg
Telephone +46 31 772 1000

Cover: Thermal contours of battery module with single cooling plate

Typeset in LaTeX
Printed by Chalmers Reproservice
Gothenburg, Sweden 2023

Time Efficient Simulations for Advanced Battery Cooling Concepts
enabling EV fast charging
SHANE SHAJU
Department of Mechanics and Maritime Sciences
Chalmers University of Technology

Abstract

The transition to electric vehicles (EVs) requires advancements in battery technology to improve range and minimize charging times. Fast charging is a key feature to enable the widespread adoption of EVs, but it presents significant thermal management challenges due to the thermal instability and higher degradation of Li-ion batteries. To address this issue, advanced battery cooling concepts are required to ensure their safety and longer lifespan. This thesis presents a method to simulate the 3D thermal behaviour of a battery module under fast charging with a given cooling strategy. This includes accurate modelling of cells to couple their electrical behaviour with thermal behaviour while considering the ohmic heating in busbars and the contribution of the cooling system. The simulation is set up in StarCCM++ using the BatterySim® tool for cell modelling. The case-study simulations are carried out on a standard battery pack with a cooling plate at the battery module's bottom. The method is verified by performing a real-time fast charging test that showed that the simulation results are in good agreement with the test data. With a 20 minutes fast charging strategy, the simulation results indicate that this cooling approach leads to a higher temperature on the top surface of the cells. Hence, the design is modified by adding another cooling plate to the top. This design effectively cools the battery with minimal temperature gradients. Another studied strategy, involving the placement of thin heat pipes between each cell, proved to be an even more effective approach as cells were cooled efficiently and uniformly. By using this method, the design of a battery module can be further optimized to have a more uniform temperature in the optimum temperature range.

Keywords: Li-ion battery, electro-thermal modelling, cooling systems, fast charging

Acknowledgements

I would like to express our sincere appreciation to everyone who helped make this thesis work in conjunction with Polestar a success. This work would not have been accomplished without their support, guidance, and provision of necessary resources.

First and foremost, I would like to acknowledge the support and guidance of my industrial supervisors, Anders Wedin and Jens Groot, as well as my academic supervisor, Petter Dahlander. Their knowledge, advice, and ongoing assistance have been invaluable in shaping and directing our study. Their extensive industrial and academic experience has helped lead us on the proper route during this journey.

I'd also like to thank Martin Petisme for his significant assistance during cell modelling, notably in the extraction of cell properties from experimental data. His knowledge and support have greatly aided the precision and dependability of our findings.

Jenny deserves special recognition for her great efforts in ensuring a smooth experience throughout this endeavour. Her meticulous planning, dedication to following industry practices, and prompt provision of all essential resources have all been critical to the success of this work.

Furthermore, we would like to thank SIEMENS for their assistance in providing us with student licenses for StarCCM+ and BatterySim®. I have been able to use these sophisticated tools in my simulations, improving the quality and depth of my analyses.

Finally, I would like to convey my heartfelt gratitude to those people whose contributions, while not expressly stated, had a vital impact on my thesis effort. Your encouragement, support, and collaboration are greatly appreciated.

Thank you all for your support and for being a part of this incredible journey.

Shane Shaju, Gothenburg, June 2023

List of Acronyms

Below is the list of acronyms that have been used throughout this thesis listed in alphabetical order:

AC	Alternate Current
BDS	Battery Design Studio
BEV	Battery Electric Vehicle
BMS	Battery Management System
CAD	Computer Aided Design
CMA	Compact Module Architecture
DC	Direct Current
ECM	Equivalent Circuit Model
EDP	Electrodynamic Potential Solver
FCV	Fuel Cell Vehicle
HEV	Hybrid Electric Vehicle
IC	Internal Combustion
IEA	International Energy Agency
Li	Lithium
NS	Navier Stokes
OCV	Open Circuit Voltage
PCM	Phase Change Material
RCR	Resistance Capacitance Resistance
SEI	Solid Electrolyte Interface
SHE	Standard Hydrogen Electrode
SOC	State of Charge

Nomenclature

Below is the nomenclature of indices, parameters, and variables that have been used throughout this thesis.

C	C-rate
C_1	Capacitance for RC element-1
C_2	Capacitance for RC element-2
C_n	Battery cell capacity
CO_2	Carbon dioxide
η	Coulombic efficiency
F	Faraday constant
g	Gravitational acceleration
$I_{batt}(t)$	Current flowing through the battery cell
k	Thermal conductivity
n	Total no. of electrons transferred per atom
∇	Del operator
P	Pressure
ϕ	Volumetric heat generation
$\dot{Q}$	Rate of heat generation
R_1	Resistance for RC element-1
R_2	Resistance for RC element-2
R_o	Ohmic resistance
ρ	Density
ΔS	Entropic change in cell
T	Temperature
τ_{ij}	Stress tensor
u	Internal energy
V	Velocity
$V_1(t)$	Voltage for RC element-1

$V_2(t)$	Voltage for RC element-2
V_{batt}	Terminal Voltage
$V_{OC}(SOC)$	Open circuit voltage

Contents

List of Figures

List of Tables

1
Introduction

Electrification of transport is seen as a viable solution to address the lower efficiency of Internal combustion engines and higher tailpipe emissions. The energy storage system, which is a critical component of an electric vehicle, plays an important role in enabling the transition towards electrification. Among the various energy storage technologies, Li-ion batteries have attracted significant attention for electric cars. This is because of their higher specific energy and longer lifespan. Li-ion batteries will not only contribute to the lower weight of these cars but will also prolong their life, contributing to overall reduced emissions.

However various research studies have uncovered peculiar characteristics of Li-ion batteries. It has been identified that temperature is one of the key parameters that affect cell ageing [1], [2]. The optimum temperature for cells ranges from $10°C$ to $40°C$. However, even in this temperature range, higher temperature gradients inside the cells lead to higher degradation [3]. The other major concern is the safety issue of Li-ion batteries. The organic carbonate-based electrolyte used in Li-ion batteries is thermally unstable even at temperatures below $100°C$ [4]. This poses a risk of thermal runaway.

For these reasons, the battery pack of an electric vehicle requires a cooling and heating system to effectively manage the temperature of the cells. Batteries generate heat during charging and discharging. This heat becomes significant during fast charging when a large amount of current has to be supplied to the cells. An efficient and effective thermal management system will transfer all the heat to the cooling system while maintaining the battery cells' temperature in the optimum range with minimum temperature gradients.

1.1 Motivation

Accurate models play an important role in addressing the challenges of Li-ion batteries and guaranteeing a safe, reliable operation and longer life of batteries in electric and hybrid electric vehicles (HEVs). These models will enable the prediction of temperature distribution and heat generation rates by offering useful insights into the behaviour of battery cells under various circumstances.

By considering the electrical characteristics of the battery, electro-thermal modelling can give more detailed insights into the battery design. Large currents during fast charging result in increased heat generation and potential thermal management difficulties. Electro-thermal modelling enables the examination of the thermal behaviour of the battery during the fast-charging event. By tweaking these models to reduce the computational cost, it will enable iterative design adjustments to optimize the thermal management of the battery system. This will ensure the safety and reliability of electric cars, contributing to their widespread adoption.

1.2 Scope of the work

This work uses a 0D RCR Equivalent Circuit Model with a single RC element to model the cell's behaviour. This model can predict the heat generation inside the cell with good accuracy considering a uniform heat generation rate inside a cell. To reduce the complexity of the model the effect of heat transfer to/from the ambient environment is neglected. For example, air is not modelled in the void spaces inside the geometry and it is assumed that all the walls are adiabatic. All the contacts are assumed to be perfect. However, a thermal contact resistance of 0.001 m^2K/W is assumed for the contact between the cooling plate and frame. To quantify the thermal behaviour of a heat pipe, it was assumed that it is behaving like a copper plate with a thermal conductivity value ten times higher.

1.3 Objectives

The objectives of the work are:

- Model the cell behaviour by incorporating the electrical and thermal models.
- Develop a Methodology to simulate a 3D CFD and electro-thermal behaviour model of a battery pack during fast charging. This should also capture the effect of joule heating in the busbars.
- Reduce computational cost by various strategies to have a good trade-off between accuracy and computational power.
- Investigate the various solutions for a more optimal and efficient cooling system.

2

Literature Review

To address the global challenge of global warming, there is a growing need to switch to renewable energy sources like wind, solar, and hydropower. However, the unpredictable nature of such resources necessitates the development of effective energy storage technologies. The growing use of modern lithium-ion (Li-ion) batteries powered electric (BEV) and hybrid electric vehicles (HEV) offers one of the viable solutions to this issue. Lithium-ion batteries offer advantages such as lightweight design, high energy density, and longer lifespan. This makes them an attractive choice for automotive applications.

Countries around the globe including Sweden, Norway, Denmark, China, and Germany are showing strong commitments to electrifying their transportation. As a result, the EV market is growing rapidly. According to International Energy Agency (IEA), the number of electric vehicles has increased by around five times in 2022 compared to 2018 [5] as shown in figure 2.1. Many major automakers including Polestar, have started campaigns to promote e-mobility and a future with net zero emissions in the next ten or twenty years [6] [7]. However, the transition to electrification of transportation also brings new challenges that must be addressed to ensure long-term adoption and long-term sustainability.

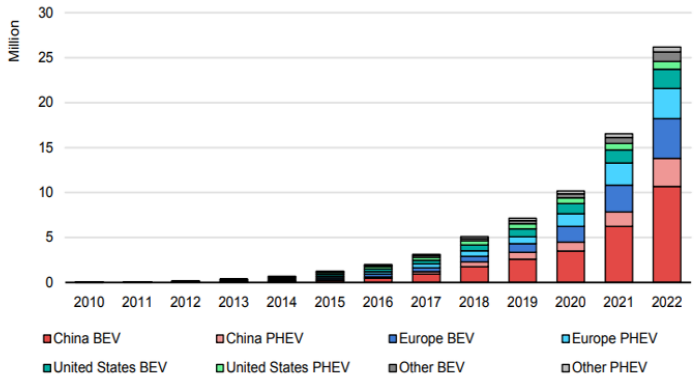

Figure 2.1: The global electric car stock 2010-2022 [5]

Li-ion batteries have gained significant attention in the market because of their higher energy density and longer lifespan. That's why all automotive companies are focusing on integrating Li-ion batteries in their production vehicles. Nevertheless, Li-ion batteries have some challenges and limitations that necessitate attention and

resolution. One of the prominent concerns is that they are thermally unstable, primarily because of combustible electrolytes. At temperatures above $100°C$, there is a risk of thermal runaway. This poses a considerable safety hazard.

Another key aspect of Li-ion batteries is their lifespan, which is influenced by several parameters. Among these parameters, temperature and state of charge (SOC) have a significant impact on cell ageing [2]. It is generally recommended to operate Li-ion batteries within the optimal temperature range $10°C$ to $40°C$ while keeping SOC between 10% to 80% to have minimum degradation. Additionally, high-temperature gradients within a cell can also contribute to higher degradation [3]. This directly affects the electrolyte and electrode chemistry which will result in poor performance of the cells. Hence, maintaining suitable temperature conditions and avoiding large temperature differentials are crucial for preserving the longevity and performance of Li-ion battery cells.

Compared to internal combustion (IC) cars, which have relatively quick fuel-filling times, EVs typically require longer charging times. Fast charging is a key feature aimed at reducing charging times for EVs. However, the rate of charging a Li-ion battery is limited by several factors and one significant limitation is the substantial heat that is generated during fast charging. This heat, if not properly managed, can significantly elevate the temperature of the battery which will impact battery performance. In the worst condition, the temperature can elevate to potentially hazardous levels, posing a risk of thermal runaway.

Using accurate models to design an efficient thermal management system can effectively tackle these challenges. An optimized thermal management system can unlock the potential of EV fast charging ensuring a high level of safety and longer lifespan. By actively controlling and regulating the temperature of the battery during fast charging, the thermal management system can effectively mitigate the risks associated with excessive heat generation. However, to efficiently design a thermal management system, accurate models are required. Different models have been developed to accurately predict the heat generated inside the cells. Equivalent Circuit Model (ECM) is widely used to model cell behaviour at a considerably good accuracy [8]. This model can accurately predict the irreversible heat inside the cells during charging/discharging. However, the more precise model will also incorporate the heat generated because of the chemical reaction inside the cell, i.e., entropic heat. Zeyang et al. have developed an efficient and cost-effective way to measure the entropic coefficient for a cell [9]. Incorporating this additional factor into the model would enhance its accuracy and provide a more comprehensive understanding of the heat generation mechanisms during battery operation. This work uses an integrative approach by integrating CFD with cells electrothermal model of a cell to simulate the module behaviour. This will enable analysing its thermal behaviour during fast charging. By incorporating the cell's heat generation, resistance heating in the busbars, and modelling the cooling system, this model can give detailed insights into the 3D temperature distribution inside the module. The proposed method is time-efficient, enabling the designers to refine the design through continuous iterations.

2.1 Electric Vehicles

Electric vehicles use electric energy as the power source instead of gasoline or diesel. This results in significantly lower greenhouse gas emissions and other pollutants. Electric vehicles (EVs) do not require an internal combustion engine since they are powered by a battery and propelled by an electric motor, resulting in almost two times higher energy conversion efficiency than conventional IC engines. Additionally, various capabilities of an electric motor, such as start-stop and regenerative braking features, can be exploited to further minimize energy losses, reducing energy consumption by 20-30% [10]. Thus, EVs can have a major contribution to cutting out our energy consumption and reducing emissions. They are classified by energy source and propulsion device as shown in figure 2.2.

- **Battery-powered electric vehicles (BEV)**: Battery-powered electric vehicles (BEVs) rely entirely on rechargeable batteries to power an electric motor and can travel up to hundreds of miles on a single charge.
- **Fuel cell vehicles (FEVs)**: Fuel cell vehicles (FEVs) use a combination of hydrogen and battery to generate electricity to power an electric motor, with water being the only by-product.
- **Hybrid electric vehicles (HEVs)**: Hybrid electric vehicles (HEVs) combine a gasoline or diesel engine with an electric motor and battery pack, allowing for greater fuel efficiency and reduced emissions. Many automotive companies are investing in the development and production of electric vehicles to meet the growing demand for sustainable transportation options [10].

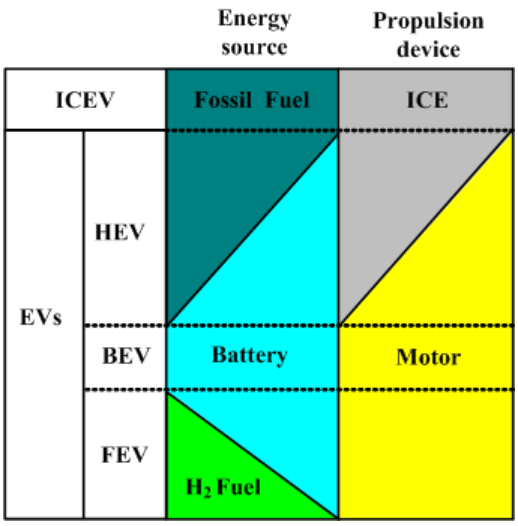

Figure 2.2: EV Classification by energy source and propulsion method[11]

2.2 Batteries

2.2.1 Chemistry of a Battery

A battery is an electrochemical device that stores energy in chemical form. This energy is then converted back into electrical form when required. A simple battery has the following 5 components: anode, cathode, current collectors, electrolyte and separator as shown in figure 2.3. Redox reactions occur at the electrodes, resulting in the movement of electrons in the external circuit.

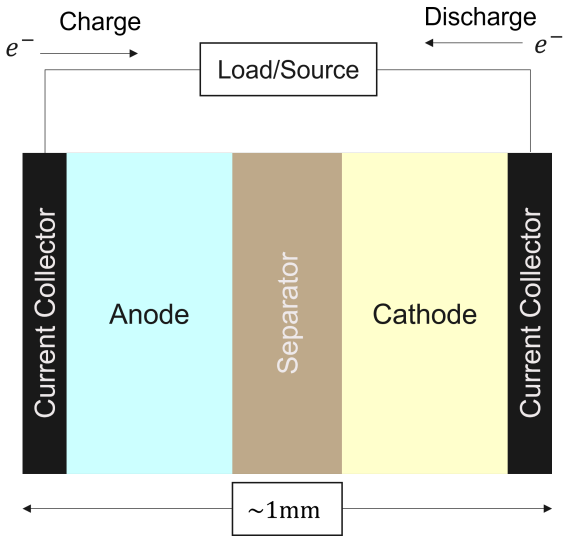

Figure 2.3: A battery cell

To store more energy, several layers of such cells are stacked together to occupy a larger volume and provide a larger surface area for current collectors. Thus, it can have several configurations e.g. prismatic, pouch, or cylindrical. A simple pouch cell is shown in figure 2.4. The stacked layers of a cell are encapsulated in a pouch that provides better mechanical strength, compact design, and good heat transfer characteristics.

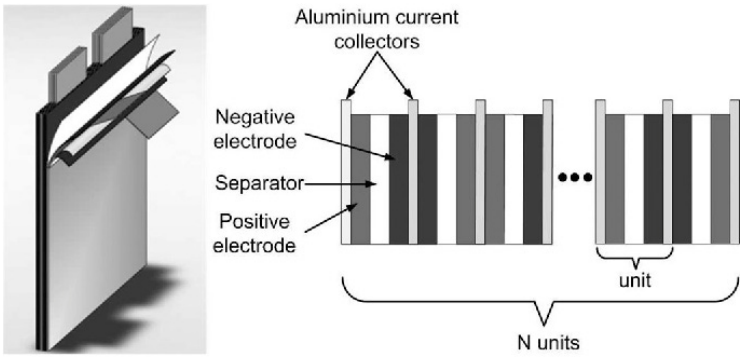

Figure 2.4: A pouch cell[12]

2.2.2 Terminology

- **Open Circuit Voltage (OCV)**: This is the difference of electrical potentials between the positive and negative terminals of a battery cell when no load is connected.
- **State of Charge (SOC)**: State of charge is the energy available in the battery compared to its to total storage capacity.
- **Terminal Voltage**: When a cell is connected with a load such that the circuit is complete, the potential difference across its two terminals is called terminal voltage.
- **Nominal Voltage**: This is the standard voltage by which a cell is referred to. During operation, the potential difference across the two terminals of a battery varies across nominal voltage.
- **Capacity**: This is the amount of charge storage capability of a cell commonly expressed in Ah (Ampere-hour).
- **C-rate**: The C-rating of the cell is the rate at which the cell is being charged or discharged. At 2C, the cell will be charged/discharged in half an hour. However, with C/2, the cell is being charged/discharged in 2 hours.

2.2.3 Cell Configurations in an EV

To power a vehicle, a single cell alone can't meet its energy requirements. Rather, multiple cells must be connected in a carefully structured manner to form a complete battery pack. This is why automotive battery packs are typically designed and manufactured in a cell-module-pack structure as shown in figure 2.5 [13]. Battery production can be mainly divided into two major stages. The first stage is focused on manufacturing a cell that involved sourcing and preparing the necessary materials to form a battery cell. In the second stage, the cells are assembled into modules and packs, which is a purely mechanical process.

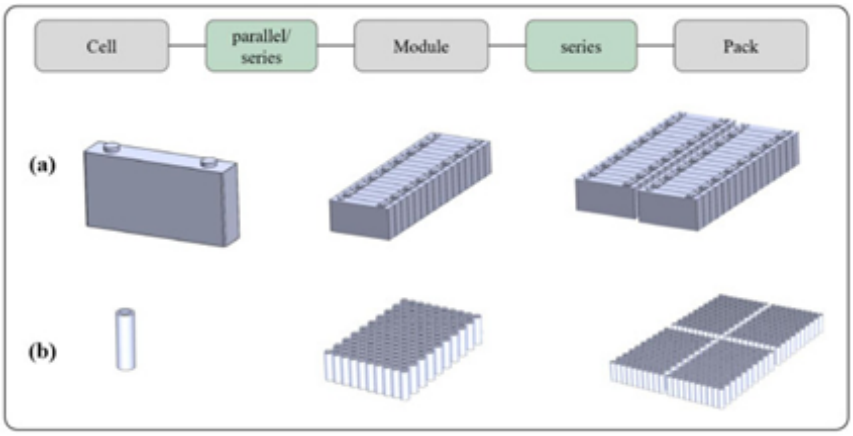

Figure 2.5: Cell-Module-Pack Schematic

2.2.3.1 Cell

A cell is a basic unit that stores chemical energy in the form of electrochemical reactions. It typically consists of two electrodes (a positive cathode and a negative anode) separated by an electrolyte. When the battery is charged, a chemical reaction occurs between the electrodes and electrolyte, which creates a potential difference that can be used to power a device. Cells are available in various geometries and configurations like pouch, prismatic and cylindrical [14]. A simple pouch cell used in this model is shown in figure 2.6. The dimensions of this cell are around $350 \times 100 \times 10mm^3$.

Figure 2.6: Pouch cell

2.2.3.2 Module

A battery module, as shown in figure 2.7 is a collection of individual cells that are combined to provide a higher voltage and capacity than a single cell. The cells in a module are connected in a series or parallel configuration, depending on the desired voltage and capacity that needs to be achieved. A 4s3p configuration means that 4 cells are connected in series and have 3 parallel connections. The battery module typically consists of a group of cells encased in a protective housing e.g., a monoframe. The monoframe is designed to provide mechanical strength and protect the cells when subjected to various types of loads. A thermal resin is placed between the cells and monoframe to create good thermal contact and to prevent mechanical damage and vibration that can lead to cell deformation and short circuits. Separate compression pads and cell tapes are placed between the cells to allow for swelling of the cells. The module also includes additional circuitry for balancing the cells' voltages and temperatures. Generally, a cooling plate is pasted at the bottom of the module to for cooling and heating the cells when needed. Achieving perfect contact between the coolant plate and the monoframe is still a challenge [15]. Generally, a thermal interface material is used that efficiently fills the gaps to achieve good contact.

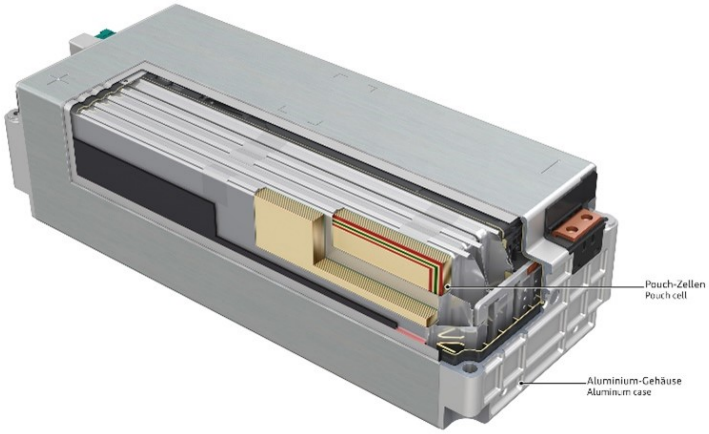

Figure 2.7: A Battery Module

2.2.3.3 Pack

A battery pack is a collection of battery modules that are connected to provide the desired voltage and capacity for an EV. A battery pack can be composed of multiple modules arranged in a series, parallel, or series-parallel configuration to achieve the desired voltage and capacity. Typically, it also includes a battery management system (BMS) that monitors the cell performance, temperature, and state of charge to ensure safe and efficient operation.

2.3 Cell Modelling

To represent the electrochemical behaviour of a cell, a simple and effective model is an RCR equivalent circuit model as shown in the figure 2.8. This model allows for the modelling of complex electrochemical phenomena in a relatively simple way, by modelling the complex behaviour of a cell into a few key parameters that can be easily measured or estimated. The cell is modelled by a voltage source, a resistor in series, and m-RC elements [8].

Typically, two RC elements are included in the model to have a good trade-off between accuracy and complexity. This circuit element model is shown in figure 2.8. The resistor R_0 stands for ohmic resistance that incorporates the resistance of the contacts, electrodes, and electrolytes. The double RC element captures the transient battery dynamics such as the charge transfer kinetics, the Li-ion diffusion, and Solid Electrolyte Interface (SEI) dynamics [16]. V_{OC} represents the open circuit voltage OCV, which is mainly dependent on the SOC of the battery. To have a good model, the dependence of each element of the cell on SOC, temperature, and current should be known. A cell can also have a different behaviour during charging and discharging.

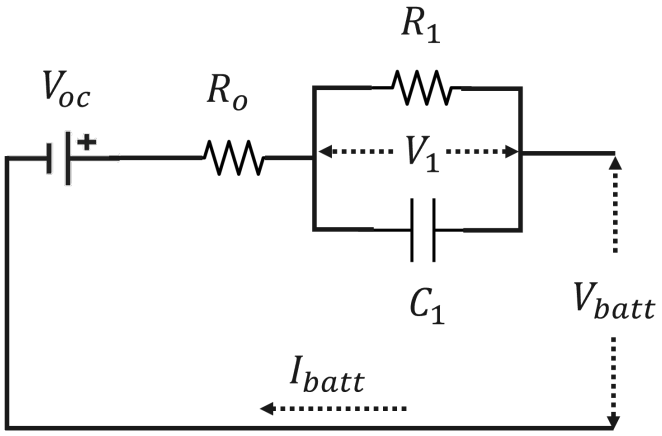

Figure 2.8: RC Model

The behaviour of this circuit can be completely described by the following set of equations [16].

$$\frac{dV_1(t)}{dt} = \frac{I_{batt}(t)}{C_1} - \frac{V_1(t)}{R_1 C_1} \tag{2.1}$$

$$\frac{dV_2(t)}{dt} = \frac{I_{batt}(t)}{C_2} - \frac{V_2(t)}{R_2 C_2} \tag{2.2}$$

$$V_{batt}(t) = V_{OC}(SOC) - V_1(t) - V_2(t) - R_o I_{batt}(t) \tag{2.3}$$

However, the SOC of the battery can be calculated by

$$\frac{d}{dt} SOC(t) = \frac{-\eta}{C_n} I_{batt}(t) \tag{2.4}$$

2.3.1 Heat Generated in a cell

The amount of heat generated in the cell can be calculated by using the governing equations of an equivalent circuit model (ECM) as discussed in section 2.3. Siemens StarCCM+ has a separate module, BatterySim® that will calculate the heat generated in the cell once its characteristics are properly defined. In normal working conditions of a cell, heat is generated as a result of entropic changes and ohmic losses. However, at higher than critical temperatures, a big portion of heat generation may come from side reactions which may contribute to thermal runaway. For the normal working of a battery, the complex heat generation inside is calculated by Bernardi's equation [17] as follows:

$$\dot{Q}(t) = I_{batt}(t)[V_{batt} - V_{OC}] + I_{batt}(t) T \frac{dV_{OC}}{dt} \tag{2.5}$$

The first term on the right-hand side of this equation is the irreversible heat generated by ohmic losses while the second term is associated with the entropic change. The term $\frac{dV_{OC}}{dt}$ is called entropic coefficient which is related to entropy change [9]:

$$\frac{dV_{OC}}{dt} = \frac{\Delta S}{\eta F} \tag{2.6}$$

Where ΔS is the entropic change in the cell, whose sign will depend on whether the cell is being charged or discharged. 'η' is the total number of electrons transferred per atom and F is Faraday's constant. Practically, the entropic coefficient is calculated experimentally since it is depending on the SOC of the cell.

2.4 Thermal Modeling

Thermal modelling is the process of developing mathematical or computational models to capture the thermal behaviour of a system[18]. It can describe the different types of heat transfer processes occurring inside the domain such as conduction, convection, and radiation, providing valuable insights into the temperature distribution. Hence, hotspots, cold spots, and temperature gradients can be visualized in a given domain. By identifying hotspots and temperature gradients the design can be refined further to efficiently manage temperature distribution in a domain. Thermal models can be used to improve efficiency, decrease waste heat, and improve thermal performance.

No model can perfectly capture all the parameters of a system. Therefore, good approximations should be made to have a good trade-off between modelling complexity and the level of accuracy. This is why a thermal model should be validated against experimental results to make it reliable.

2.4.1 System under consideration

The system in context, is shown in figure 2.9. Heat is generated inside the cells during charging and discharging. This heat is conducted to the low-temperature coolant that flows inside the coolant plate at the bottom, which is convected away be the coolant to the ambient. One of the issues in assembling metallic parts is that it can significantly impact heat transfer. This is because of the imperfect contacts between metallic parts that offer higher resistance to heat conduction. For this reason, a thermal resin is placed between the cells and frame to provide a better path for heat conduction. Similarly, a thermal interface material is used between the frame and coolant plate to effectively reduce the thermal barrier.
From a computational point of view, the coolant region can be quite challenging. This is because to solve the fluid thermally, NS-equations also need to be solved along with the energy equation. This computational effort for liquid coolant increases exponentially with the flow rate. Comparably in the solid region, only the energy equation needs to be solved; with much lower computation. The NS equations and the energy equation in their differential form are written as [19].

$$\frac{\partial \rho}{\partial t} + \nabla \cdot (\rho V) = 0 \tag{2.7}$$

$$\rho \frac{DV}{Dt} = \nabla \cdot \tau_{ij} + \rho g = \nabla P \tag{2.8}$$

$$\rho \frac{du}{dt} + P(\nabla \cdot V) = \nabla \cdot (k \nabla T) + \phi \tag{2.9}$$

Thus there are three equations and five unknowns ρ, V, P, T, u. However, the density ρ and internal energy u can be expressed in terms of pressure and temperature which constitute the set of equations. The term ϕ accounts for the source of heat generation. When coupling the electro-thermal behaviour of the battery, the heat generation term comes from the solution of the governing equation of the RCR equivalent circuit model and is calculated through Ohm's Law. In the busbar region, this heat is generated because of the electrical resistance of the material that is calculated by the solution of Maxwell's equations [20] to solve for the electric field and current distribution.

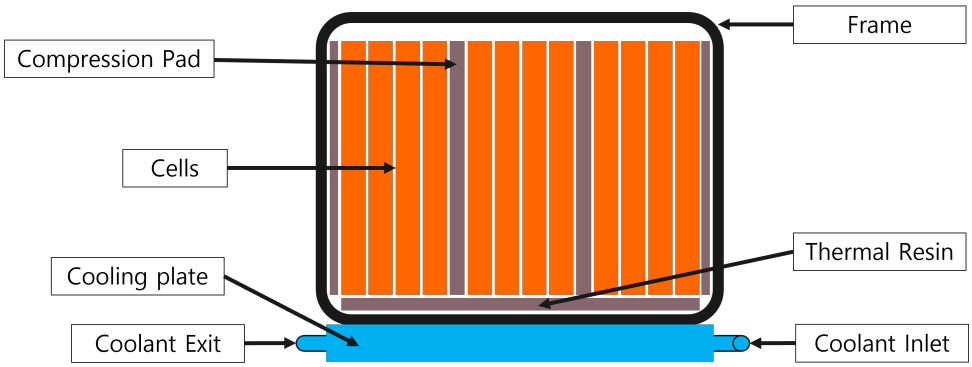

Figure 2.9: Schematic of a single battery module with a cooling plate

2.5 Existing cooling strategies for EV battery packs

Battery cooling is an important aspect of electric cars and it is essential for maintaining the safety, overall longevity, and performance of battery packs. In current electric vehicles in production, there are multiple options available for cooling like air cooling, liquid cooling, liquid immersion cooling, active thermal management systems and Phase change materials (PCMs).

2.5.1 Air cooling

Air cooling is a common cooling strategy used in EVs. It can either be passive air cooling or active air cooling [21]. Passive air cooling relies on the preexisting airflow or fans present in the vehicle to cool the battery pack, whereas active air cooling makes use of specialized fans or blowers to further increase the cooling efficiency.

Air cooling systems are relatively cheap and require low maintenance, however, they might not work optimally for high-temperature applications like battery pack fast charging.

2.5.2 Liquid cooling

In comparison to basic air cooling, liquid cooling can provide more efficient cooling. The heat from the cells produced during charging or discharging is removed by the flow of coolant which is in contact with the cells. The coolant generally flows in a cooling plate. Another application is the use of heat exchangers to move heat away from the battery pack. Generally, liquid cooling systems provide sufficient cooling performance even during DC fast charging scenarios. They can be more expensive than their comparative air-cooled systems due to the additional equipment like radiators and pumps.

2.5.3 Phase change materials (PCMs)

PCMs are another innovative alternate cooling option. During phase transitions, these materials absorb and release significant amounts of latent heat [22]. The excess heat produced during fast charging can be removed by the PCM. Therefore, this kind of cooling system provides efficient, lightweight cooling for the battery pack. A few of the available PCMs are paraffin wax, salt hydrates, organic compounds, metal alloys, etc. The disadvantages of PCMs however would be the requirement for sufficient space within the pack and the gradual degradation of these materials over time.

2.5.4 Active thermal management systems

Active thermal management systems regulate the temperature of the battery pack using a combination of heat pumps, liquid cooling, PCMs and control strategies [23]. This is achieved by actively monitoring and adjusting the battery temperature using sophisticated control algorithms and sensors. These systems provide the best thermal management solution which would be effective in various driving conditions and help improve battery efficiency[24].

In conclusion, multiple cooling techniques are used by current electric vehicles for their battery packs. Liquid cooling offers more efficiency and more accurate temperature control whereas air cooling is a common and affordable alternative. Passive cooling is provided by phase change materials, while advanced temperature control is offered by active thermal management systems. The best cooling approach depends on several parameters, including power requirements, cost concerns, vehicle architecture, and intended performance goals. Each strategy has pros and downsides. For additional improvements in EV battery cooling, future research and development activities will focus on enhancing cooling methods, optimizing system designs, and integrating cooling systems with vehicle energy management.

2.6 Meshing

While developing thermal models, it is needed to have a temperature distribution at each location in the domain. Therefore, the domain is divided into smaller and simpler geometric shapes called computational cells, or elements. The meshing generated some parts is shown in figure 2.10. This serves as a framework for numerical methods to solve the governing equations by discretizing them into algebraic equations. The algebraic equations are then solved for each cell. The accuracy of the result will of course depend upon the order of discretization of governing equations and mesh quality. A mesh can be structured in such a way that it contains regularly shaped cells, unstructured with arbitrary shapes. A good strategy is to have a hybrid mesh that uses a combination of both structured and unstructured.

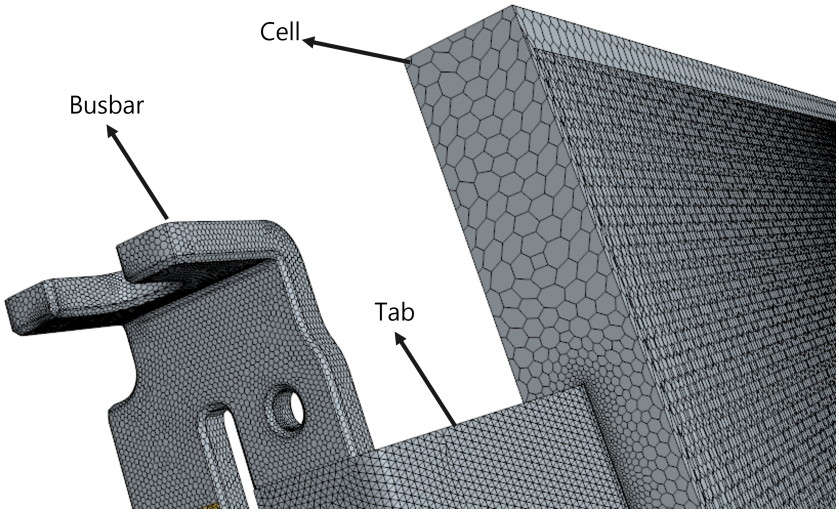

Figure 2.10: Mesh for cells, tabs and busbars

2.6.1 Validating the mesh

A "perfect" mesh for a given domain means an infinite number of cells with dimensions approaching zero. However, this is practically impossible because an infinite number of cells would require infinite computational resources, making it unfeasible to solve the problem. On the other hand, reducing the number of cells would compromise the accuracy of the results.

To achieve a balance between accuracy and computational efficiency, a suitable mesh size should be identified for a given domain. Increasing the mesh size can make the results deviate slightly from the actual values. This is because a coarser mesh may not capture all the fine details and variations in the domain, leading to some level of approximation. Therefore, it is essential to find a compromise between accuracy and computational cost.

One good approach to validate the mesh is to perform mesh dependence analysis by running the simulation iterative with different mesh sizes. This analysis can help find the minimum number of cells or mesh size for the given geometry to produce sufficiently accurate results. However, this can be time-consuming for an unsteady phenomenon or a complex geometry with multiple parts.

Another good approach is to compare the simulation results against experimental test data. This can verify that the results being generated are accurate and the methodology used to model the system is correct. However, experimentation can be time-consuming and expensive sometimes.

Some software like StarCCM+ provides different indicators for a mesh that visualize mesh quality. Some of them are explained below.

2.6.1.1 Cell Quality

A cell quality metric is an algorithm that uses Gauss and the least-square method for cell gradient calculation [25]. It not only considers the distribution of cell centroids but also the faces of the cells. As shown here in figure 2.11 [26], flat cells with highly non-orthogonal faces are considered as bad cells.

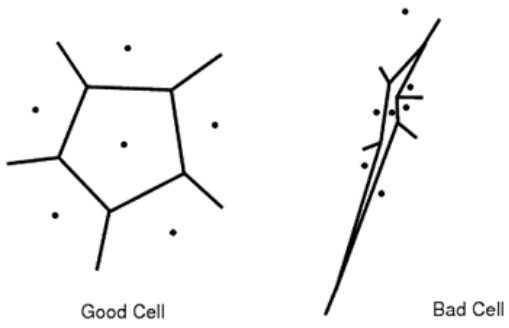

Figure 2.11: Cell Quality Metric

2.6.1.2 Volume Change

This metric is based on the fact that a sudden increase or decrease in mesh volume leads to higher inaccuracies and instability in the solvers. It calculates the ratio of the volume of a cell to its largest neighbouring cell. As shown in figure 2.12, larger volume changes are often discouraged while meshing.

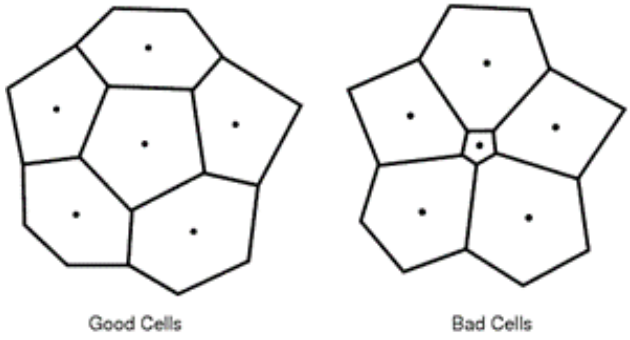

Figure 2.12: Volume Change Metric

2.6.1.3 Skewness Angle

The skewness angle of two cells is the angle between the line passing through the centroid of the cells and a line normal to the face which is common to both the cells, shown in figure 2.13. This measure ensures that there is no unbounded diffusion [26]. A cell is commonly considered bad if this angle is greater than 85 degrees.

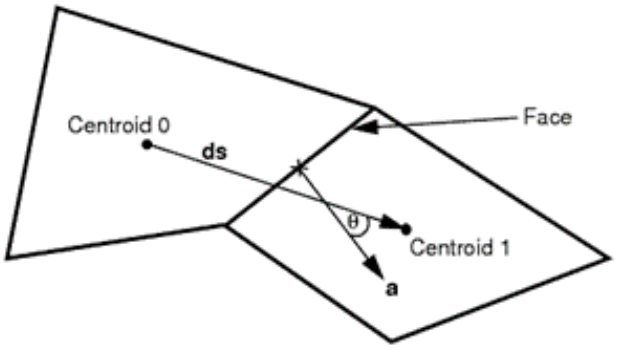

Figure 2.13: Skewness Angle Metric

2.6.1.4 Face Validity

This metric measures how the face normal for each face is oriented relative to their centroid, shown in figure 2.14. A good cell will have all its faces normal orthogonal to the faces. However, if there is some form of concavity, the value of face validity for such a cell will be lower than 1 [26].

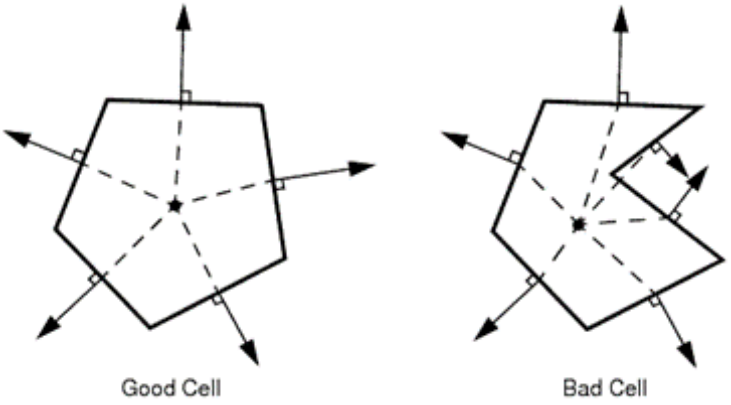

Figure 2.14: Face Validity Metric

2.6.1.5 Chevron Quality

Chevron cells are a pair of cells whose line joining the centroid of the cells doesn't pass through their face as shown in the figure 2.15. In StarCCM+, the chevron quality of a perfect mesh will be one. However, if there are chevron cells in the mesh, the value can be lower than one.

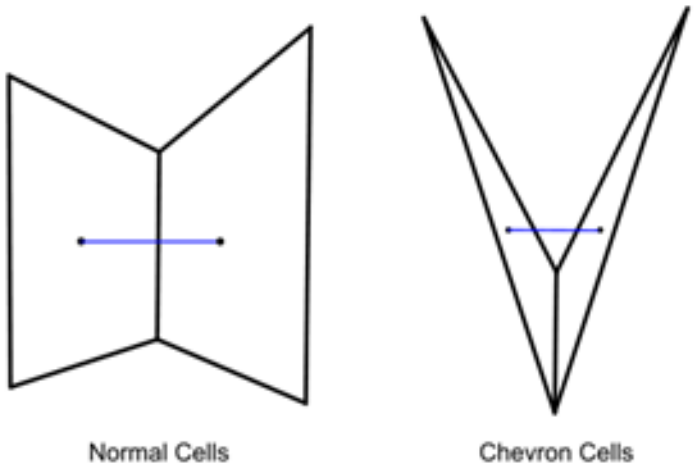

Figure 2.15: Chevron Quality Metric

3
Methodology

Every CFD simulation run on computer software has the following three steps in general. For this case, the different steps are shown in figure 3.1.

- Pre-processing
- Processing
- Post-processing

The pre-processing is the most important step as it takes a large human effort. It should be ensured that the model is set up correctly and the assumptions made in the model are valid enough that the accuracy is not compromised in the results. In this case, it was confirmed that there are no defects in the geometry and the mesh is fine enough to capture all the results with good accuracy. The important step is 'Cell-Modelling', i.e. using the right model for the cell and incorporating ohmic heating in the busbar region.

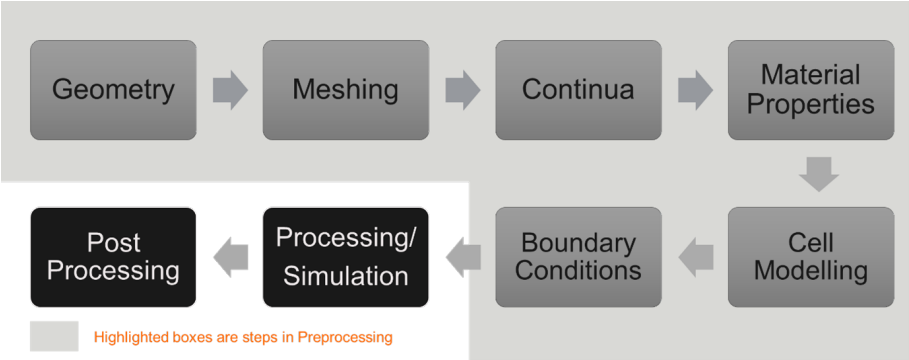

Figure 3.1: Steps in methodology

3.1 The Geometry

To develop the methodology for simulating the electro-thermal behaviour of a module, a reference geometry was used, as shown in figure 3.2. This module is being used in Polestar 2 car that is already in production since 2022. The complete geometry of this module is shown in the figure. A coolant plate, with a coolant channel, is attached at the bottom of the module to absorb the heat generated from the battery. To provide mechanical support and protection, a monoframe and the endplate cover the whole assembly of cells and busbars. To take the electric charges in or out of the cells, busbars are used which connect to the cells through leads and tabs. Because of the very high current, busbars are made thick to reduce the ohmic losses. The

cells are connected electrically in a 4s3p configuration. This means that there are a total of 12 pouch cells with 4 series connections of 3 parallel cells. Compression pads are also present between the cells to absorb shocks and allow for swelling of the cells. A thermal resin is also placed at the bottom of the cells and monoframe.

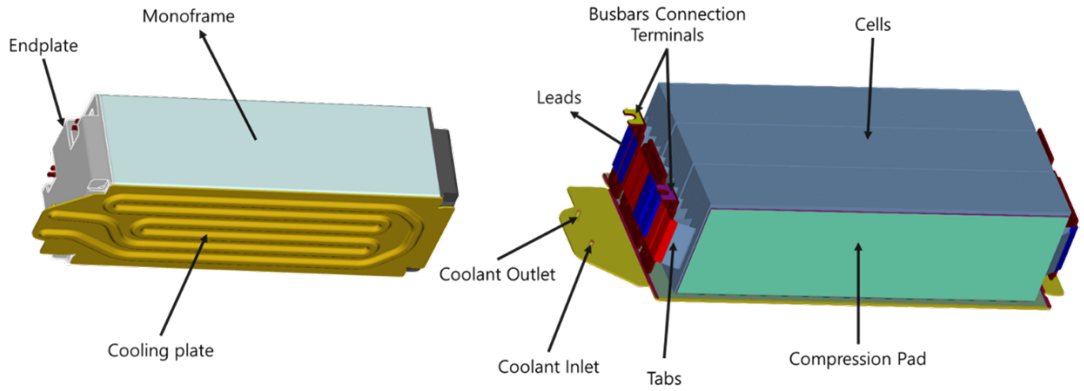

Figure 3.2: Battery Module CAD

3.2 Geometry Clean-up

Geometry clean-up is the adaptation of a 3D CAD model to make it compatible with CAE software. For example, the CAD model may have been created in Solidworks, whereas the simulation needs to be carried out in ANSYS fluent. Performing geometry clean-up helps improve the quality and accuracy of the simulations while removing certain geometry defects like gaps, free faces and overlapping faces. This also involves removing unnecessary curves and holes in the geometry to make a smooth mesh and reduce the computational cost at an acceptable level of accuracy.

In this model, the clean-up was done using ANSA to remove unnecessary details like company logos and markings, complex parts, and holes. Separate surfaces common to two different parts were also created to create better interfaces while performing the thermal simulations on StarCCM+. For example, surfaces between "cell/cell" and "Monoframe/cooling plate" define the type of interaction between the respective parts. This kind of clean-up operation helps reduce file size and makes the model easier to handle during the meshing stage which greatly helps in bringing down the computational time and resources required.

3.3 Meshing

The idea of meshing is to divide the whole geometry into smaller volumes. This way the governing equations are discretized, and the resulting algebraic equations are solved for each of the smaller mesh volumes. A very small mesh size will increase the computational cost, though it gives higher accuracy. The approach in this case was to have an optimal mesh size and get a nice trade-off between accuracy and computational cost.

3.3.1 Mesh Optimization

For this geometry, the automated mesh was generated for all the parts in StarCCM+. Most of the parts like tabs, leads, cells, and Monoframe are thin. Therefore, *thin mesher* was used for meshing such parts. For the tabs, lead and some cells, *triangular mesher* were used because of their simpler and structured geometry. However, all other parts like monoframe, busbars, coolant, and thermal resin are meshed with polyhedral cells. The coolant was a critical part in this case since the fluid flow needs quite fine resolution. *Prism Layers mesher* was also used for meshing the coolant. To ensure the quality of the mesh, several metrics like cell quality, skewness angle, face validity, volume change, and chevron quality were checked in StarCCM+ to identify bad cells. Based on the results the setting like base size, proximity refinement, and surface control were changed to mesh again. After several trials and errors, an optimized mesh was achieved that has zero *bad cells*. The mesh quality indicators are shown in Appendix A.2.

3.4 Continua

Four different continua are defined for this case by using the models available in StarCCM+. The models used for each continuum are stated in table 3.1. Each continuum is named based on its thermal behaviour.

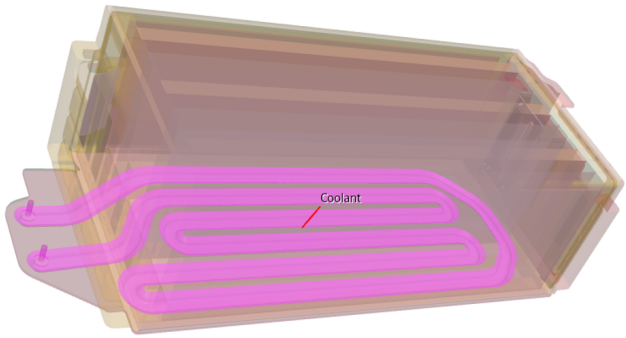

Figure 3.3: Model with coolant region highlighted

Fluid: This is defined for the coolant that flows inside the coolant plate as seen in figure 3.3. Laminar, liquid, and segregated flow models are used to capture the coolant flow since the flow rate is very low. The segregated flow solver is frozen after the initial 5 seconds of physical time to speed up the simulation. This is because the coolant flow is laminar, and the flow develops quickly within approximately 5 seconds of entering through the coolant inlet section. It would not have been possible to freeze the fluid solver if the flow was turbulent. The flow might not stabilize even after several minutes of flowing through the coolant region. To emulate the density values, the "Polynomial density" model was used since the values of coolant density change with respect to temperature.

Stacks: This continuum is defined to capture the behaviour of the cells in the module, figure 3.4. Since the electric current is also passed through this region, the "Electrodynamic Potential" model is also used. Ohmic heating is turned off in this region because the heat generation is calculated from cell modelling. The "battery" model used here activates the BatterySim® tool that enables the modelling of the electro-thermal behaviour of battery cells. An electro-thermal model helps in calculating the heat generation rate in the cells for a given current. The circuit is then modelled to replicate circuit elements and their connections using the "circuit" model mentioned in sec 3.7.

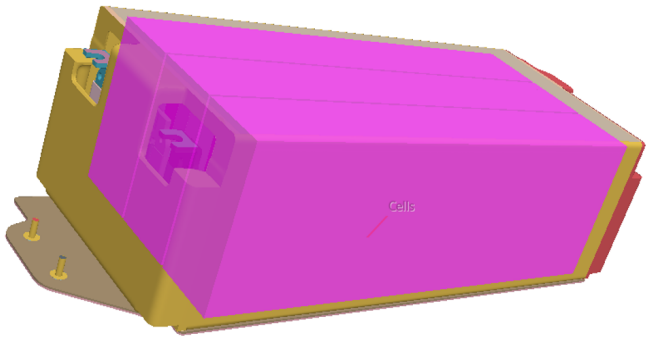

Figure 3.4: Model with stacks region highlighted

Solids-Thermal: This continuum is defined to capture the behaviour of all the solid parts that act as a thermal bridge for conducting the heat, figure 3.5 . This includes a monoframe, thermal resin, cooling plate, and compression pads.

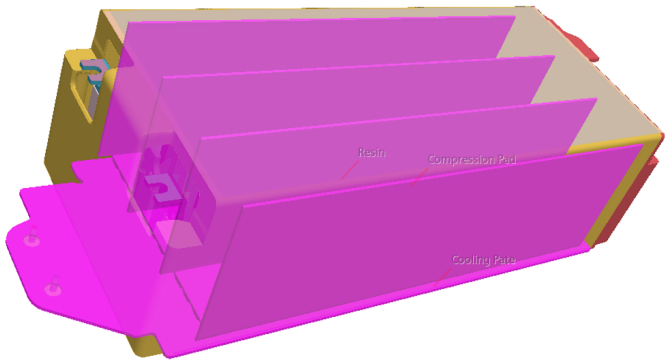

Figure 3.5: Model with solids-thermal region highlighted

Ohmic Heating: This continuum incorporates all the models employed in the 'Solid-Thermal' region to analyze heat conduction, figure 3.6. Notably, it accounts for the generation of ohmic heat by calculating the electric field across various regions. Hence, additional models such as the 'Electrodynamic Potential Solver,' 'Electromagnetism,' and 'Ohmic Heating' are also utilized.

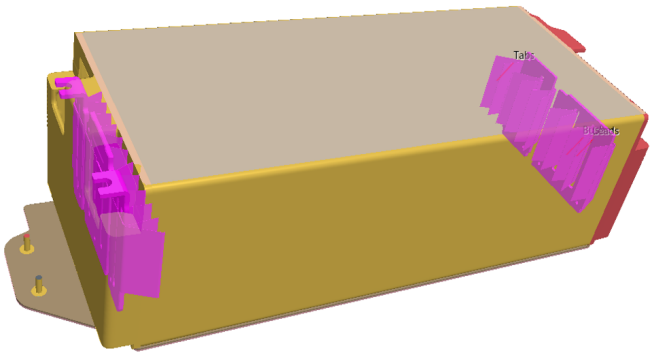

Figure 3.6: Model with ohmic-heating region highlighted

Table 3.1: Models under each continuum

Fluid	**Stacks**	**Solid-Thermal**	**Ohmic-Heating**
Cell Quality Remediation	Cell Quality Remediation	Cell Quality Remediation	Cell Quality Remediation
Gradients	Gradients	Gradients	Gradients
Implicit Unsteady	Implicit Unsteady	Implicit Unsteady	Implicit Unsteady
Three Dimensional	Three Dimensional	Three Dimensional	Three Dimensional
Solution Interpolation	Solution Interpolation	Solution Interpolation	Solution Interpolation
Liquid	Multi-part Solid	Multi-part Solid	Multi-part Solid
Laminar	Multi-component Solid	Multi-component Solid	Multi-component Solid
Segregated Fluid Temperature	Segregated Solid Energy	Segregated Solid Energy	Segregated Solid Energy
Polynomial Density	Constant Density	User Defined EOS	Constant Density
Wall Distance	Electrodynamic Potential	-	Electrodynamic Potential
Segregated Flow	Electromagnetism	-	Electromagnetism
-	Circuit Model	-	Ohmic Heating
-	Battery	-	-

3.5 Regions

The specific continuum characteristics defined above are then assigned to the geometry under consideration. This will make respective geometric parts behave according to the continuum models and the assigned material properties. The geometric parts for each of the continua are summarized in table 3.2.

Table 3.2: Parts under each continuum

Fluid	Stacks	Solid-Thermal	Ohmic-Heating
Coolant	Cells : 1-12	Coolant Plate	Busbars
-	-	Frame and Endplates	Cell tabs and leads
-	-	Compression Pads	-
-	-	Thermal Resin	-

3.6 Material Properties

Each continuum can have more than one part. To quantify the behaviour of a specific part, the material properties of the corresponding parts need to be assigned in the geometry. The property of each material part is summarized in the following table. It is assumed that the material property has no spatial dependence except for the cell's anisotropic thermal conductivity. The cell has a value of 2 W/m-K in the lateral direction and 20 W/m-K in the longitudinal direction.

The behaviour of all the parts except coolant is completely defined by fixing the three properties i.e., density, specific heat, and thermal conductivity. However, for the parts in the region of "Ohmic Heating", electrical conductivity also needs to be defined to be able to calculate the ohmic losses in those areas.

The coolant is a mixture of water and glycol whose properties are highly dependent on temperature. The temperature-dependent behaviour of the coolant is shown in figure 3.7.

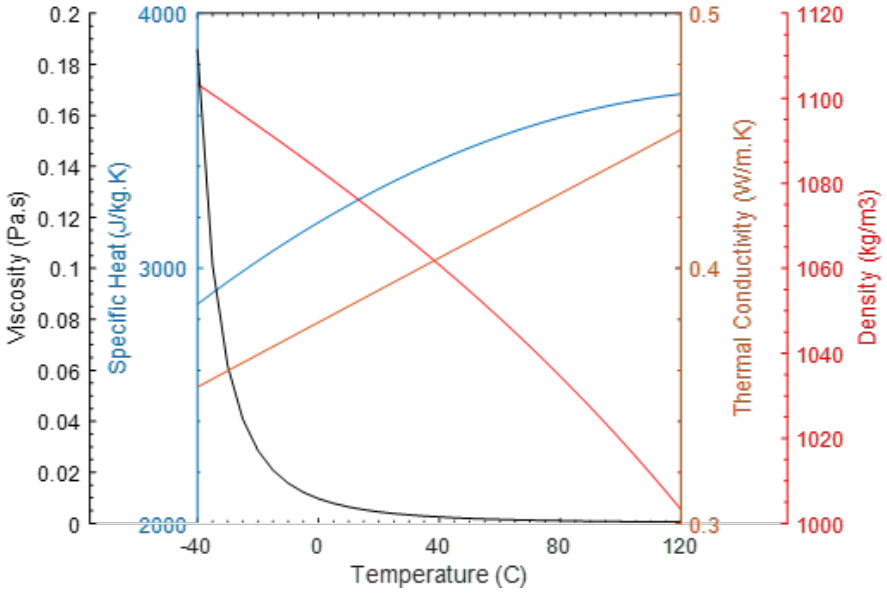

Figure 3.7: Coolant Properties

3.7 Cell Modelling

The cells used in the module have a nominal capacity of 66.4Ah. The model is set up with a single RC element as shown in figure 3.8. This is a much simpler model but here the goal is to calculate the heat generation rate inside the cells. Since this model can capture heat generation in the cell at quite good accuracy, that's why it is sufficient. The DC-IR data of the cell, from the HPPC test, is used to fit the data and extract the key parameters for this model. It was assumed that the extracted parameters are only dependent on temperature and SOC. This included finding how V_{OC}, R_0, R_1 and C_1 are changing with respect to temperature and SOC. For this method, the time constant was fixed at 30s and the other two parameters i.e., R_0 and R_1, shown in figure 3.9, are calculated by fitting to the experimental data. The data for open circuit voltage V_{OC} as shown in the figure 3.10 is measured experimentally using a voltmeter. An interesting behaviour can be noted here that the resistance of the cells is decreasing with the increase in temperature.

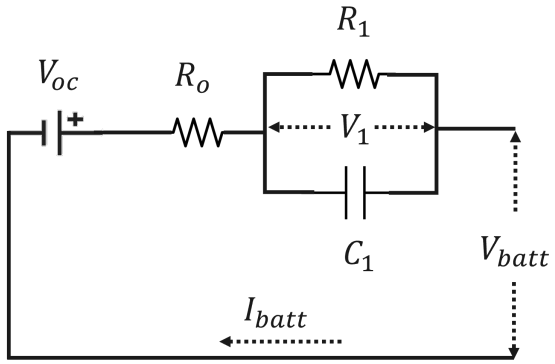

Figure 3.8: Model setup with single RC element

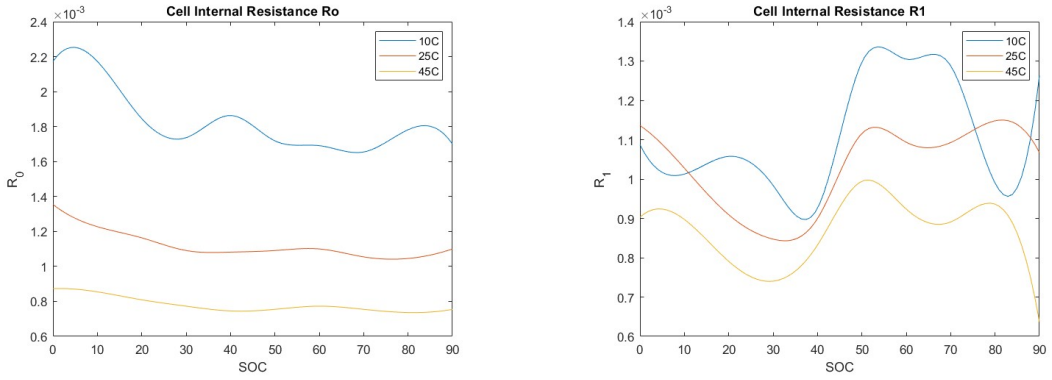

(a) Resistance R_0 **(b)** Resistance R_1

Figure 3.9: Cell Internal Resistance

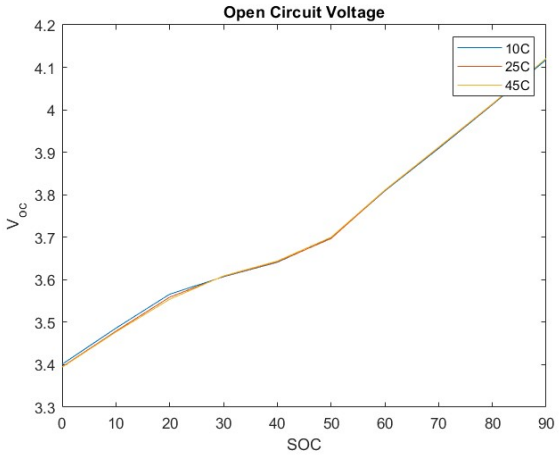

Figure 3.10: Cell open circuit voltage

3.7.1 Modelling Heat Generation

The heat is generated in the cell because of two different effects.

- Resistance losses
- Entropic Changes

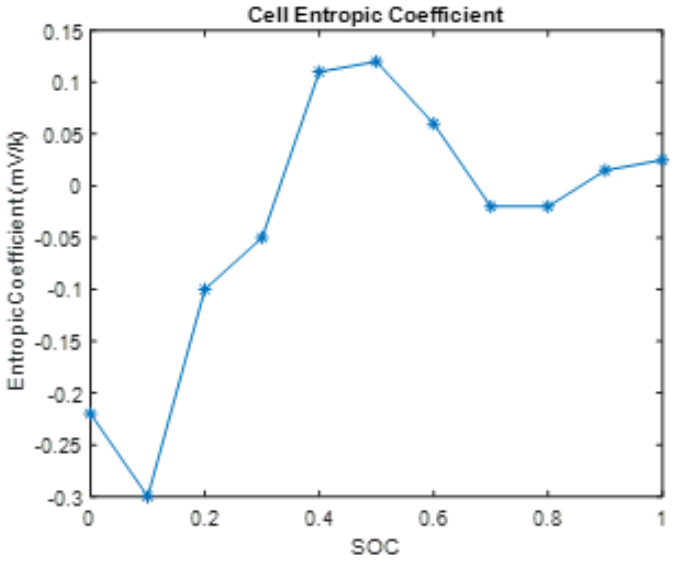

Figure 3.11: Cell entropic coefficient vs. SOC

$$\dot{Q}_{total} = \dot{Q}_{irr} + \dot{Q}_{rev} \tag{3.1}$$

$$\dot{Q}_{total} = I_{batt}(V_{batt} - V_{oc}) + I_{batt}T\frac{dU}{dt} \tag{3.2}$$

where I_{batt} is the current flowing through the battery. The irreversible heat can be calculated by solving the governing equations of a cell. However, to calculate the reversible heat, the entropic coefficient $\frac{dU}{dt}$ should be known. The entropic coefficient of the cell is dependent on the SOC of the cell which is measured experimentally. Since data for the entropic coefficient of the cell is not known, the data available in the literature for a cell of similar chemistry was used. Geng et al. [27] conducted experiments on a cell of similar chemistry to measure its entropic coefficient as shown in figure 3.11. The same data was used for this model.

3.7.2 Generation of Charging Curve

The simulations are performed by fast charging the module for 20 min by increasing its SOC from 10% to 80%. For this purpose, a specific charging curve needs to be generated as an input. Realistically, this curve is not meant for this specific module as it is recommended to charge it in 38 mins for the same increase in SOC. The fast-charging curve is generated by a trial-and-error method using the BatterySim® tool in StarCCM+. A single cell is set up, and a random charging curve (current vs time) is then applied. The corresponding cell voltage and the SOC is monitored during the charging time. It was ensured that the voltage of the cell stays below 4.2V for safety reasons. After several tries, the charging curve is optimized and the charging profile shown in figure 3.12 is obtained. The corresponding monitors of cell voltage and SOC are also shown in figure 3.13. Since three cells are connected in parallel, the module current is calculated by multiplying the single-cell current by three.

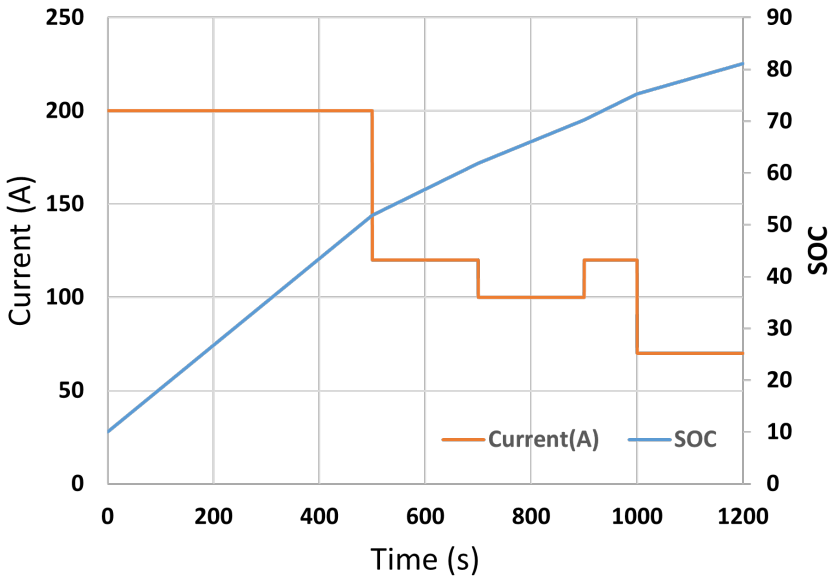

Figure 3.12: Fast charge curve with SOC variation

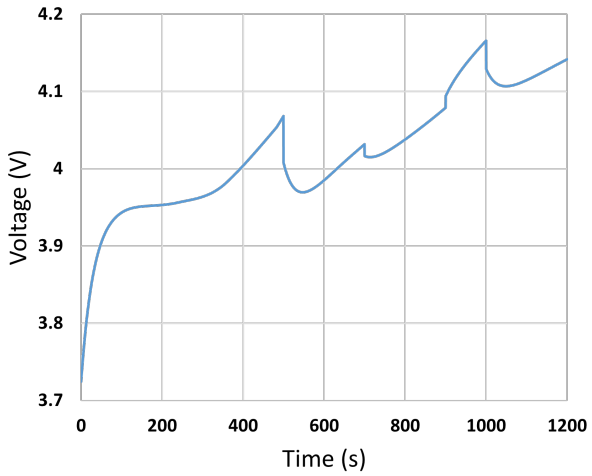

Figure 3.13: Cell voltage during fast charging

3.8 Incorporating Ohmic Heating

During fast charging, there is a need to supply a significant amount of current (for ex: 200A) to the cells. For this reason, there is significant heat generation in the busbars and tabs because of ohmic losses. To be able to consider the heating of busbars and tabs, a current is made to flow through this region and the electric field should be calculated through an electrodynamic potential (EDP) solver. This means that the BatterySim® and EDP solver should be able to communicate with each other to make the exact current flow through the busbar/tabs that the corresponding cell is facing. There is some limitation even in the latest version of StarCCM+, version 2302 where these solvers cannot communicate with each other. To solve this challenge, another current was made to flow through from the positive terminal of the busbar through tab, cells until the negative terminal of the busbar, figure 3.14. It is needed to make this current flow through the cells because it is going to provide an open path for the current. Hence the cell's region experiences two currents flowing i.e., one to incorporate ohmic heating in the busbar region and the other to calculate the heating generated in the battery according to the cell behaviour. The two currents are the same and the ohmic heating is turned off in the cell region. The same method is recommended by the support team at SIEMENS [28]. This method will have more uncertainties in results if the differences in current flowing through each cell are larger. This can occur mainly when the cells have different average temperatures. In practice, the differences should usually be negligible, so it is a good compromise.

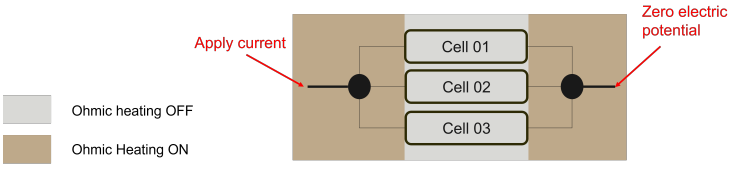

Figure 3.14: Modelling Ohmic losses in busbar/tabs

3.9 Cooling Strategies

Batteries generate a considerable amount of heat during fast charging. Therefore, an efficient cooling system is needed to reject this heat and maintain the batteries at a constant temperature. The design of the module is modified from a thermal view with several iterations to have a more even cooling of the batteries. This was a bit time-consuming process since the simulation has to be set up in the software and based on the results, the module is redesigned and cleaned using ANSA to prepare it for the simulation again. Three different design strategies were used (figure 3.15), and it was seen that each new design provided a good cooling of the cells, and we had a more even temperature distribution.

3.9.1 Design A

This is the default method which consists of a cooling plate at the bottom of the module. This design is simple and cost-effective, already present in several EVs on the market. This is the design currently in use in the Polestar 2. However, during fast charging, the top surface of the cells remains hot. This results in poor cooling of the cells.

3.9.2 Design B

To address the issues encountered with design A, an enhanced cooling solution was implemented for the battery module. An additional cooling plate was introduced, strategically positioned on the top surface of the module. This addition aimed to alleviate the previously observed uneven temperature distribution. By incorporating two cooling plates, symmetrically located at each end of the battery module, a more balanced temperature profile was achieved.

The inclusion of the additional cooling plate effectively mitigates the challenges posed by design A, thereby enhancing the overall thermal management of the battery module. The presence of dual cooling plates not only promotes improved heat dissipation but also results in a lowered average cell temperature.

3.9.3 Design C

After conducting simulations for designs A and B, it has been observed that certain areas within the cells experience high temperatures. This occurrence can be attributed to the significantly lower thermal conductivity of the cells in the direction along their thickness. Consequently, hotspots tend to form at the centre region of the module. To address this issue, the incorporation of metallic inserts between the cells presents an interesting solution. These inserts facilitate an efficient pathway for heat transfer to the coolant.

The heat pipes are strategically positioned between the cells and on the top surface. They comprise a wicking structure with water situated within them. As heat arises

from the cells, a phase change takes place, allowing the resulting vapours to rise towards the cooling plate. Subsequently, the vapours condense back into liquid water, aiding in the reduction of cell temperatures even further compared to designs A and B. However, for the sake of simplicity, it is assumed that the heat pipes operate without any fluid present and possess a thermal conductivity of approximately ten times that of copper.

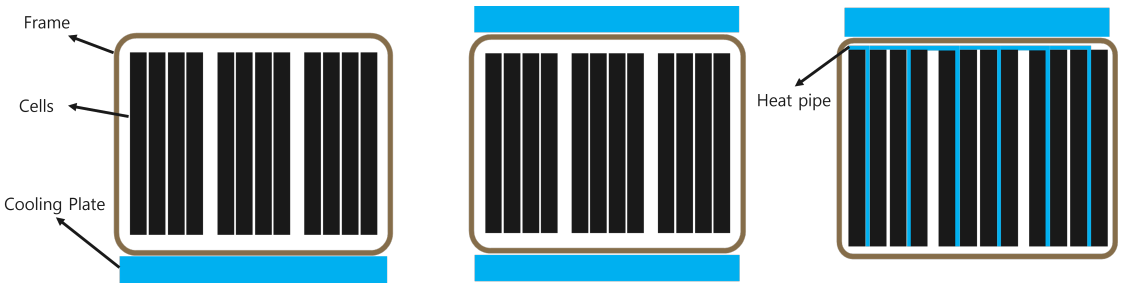

Figure 3.15: Cooling strategies for designs A, B, and C

3.9.3.1 Modelling a Heat pipe

A heat pipe is a simple device that is used to transfer heat from one location to another using the principle of phase change. The working fluid goes through a cycle of evaporation, conduction, and condensation. As a result, the overall thermal conductivity is several times increased. The simulation of the phase change phenomenon for a fluid to be quite expensive computationally. As a result, a quick way to model its behaviour is to model assume it to be like a plate of copper with a thermal conductivity ten times greater than that of copper. However, this is not a perfect model as there is a limit to the maximum heat transfer. This a because the working fluid can't exceed a maximum mass flow rate while working.

3.10 Initial/Boundary Conditions

To compare the results for the three designs effectively, the initial conditions for all three cases were kept the same. They are summarized in the following table 3.3. In all three cases, it was assumed that there is no heat transfer to the external environment and the busbars and cell tabs have adiabatic wall condition.

Table 3.3: Initial boundary conditions

Initial temperature of module	$+25°C$
Timestep	0.5 s
Max. inner iterations	10
Coolant inlet temperature	$+25°C$
Coolant mass flow rate	0.04416 kg/s (2.5 lpm)
Contact resistance	$0.001 m^2K/W$
Initial cell SOC	10%

3.11 Computational Effort

The module geometry under consideration contains significant details and several parts, meshing generates a large number of cells (figure 3.16). To emulate the flow of the coolant liquid in the coolant plate, it is recommended to have a fine mesh to help resolve all parameters accurately. For the whole geometry, a total of around 9 million cells are generated. The distribution of cells in each region is shown in the chart. The coolant contains around 45% of the total number of cells which makes it quite expensive computationally.

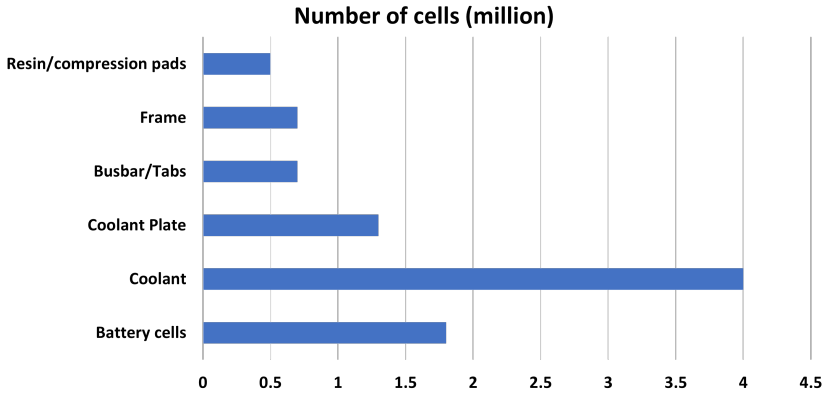

Figure 3.16: Number of cells for each meshed part

3.11.1 Reducing the computational cost

Running the simulations for design A took around 28 hours on a cluster with 120 cores and 440GB RAM. In this case, all the solvers were solving the corresponding fields throughout the charging time. This included solving the flow field for the coolant, the electric field in the region where the current is flowing, the governing equations for a cell, and heat conduction in all other parts. The timestep of 0.1s is used with 10 inner iterations in each timestep. Several strategies were implemented to reduce the computational effort. As a result, the total computational time was reduced to around 2.5 hours.

3.11.1.1 Freezing the flow solver

The coolant flows in the pipe that has more like a rectangular cross-section. In this method, the simulations are run for five seconds, in the beginning, to allow the flow to develop in the coolant channel. Now the 'segregated flow solver' is frozen. This way the already developed velocity field will be used for the next timesteps. Hence, the effort of solving the flow field at each time step is reduced. This reduced the computational cost by 4 times.

3.11.1.2 Increasing the timestep

Instead of using the timestep of 0.1s, a 0.5s timestep is used. The cell temperature is noted down and compared together for both cases. It can be seen that the cell's average, maximum, and minimum temperature are almost identical for both cases and there is no significant effect on the results, figure 3.17. During the peak temperature time, there is a slight difference between the maximum temperatures for both cases. But this effect can be neglected as its overall effect is less significant.

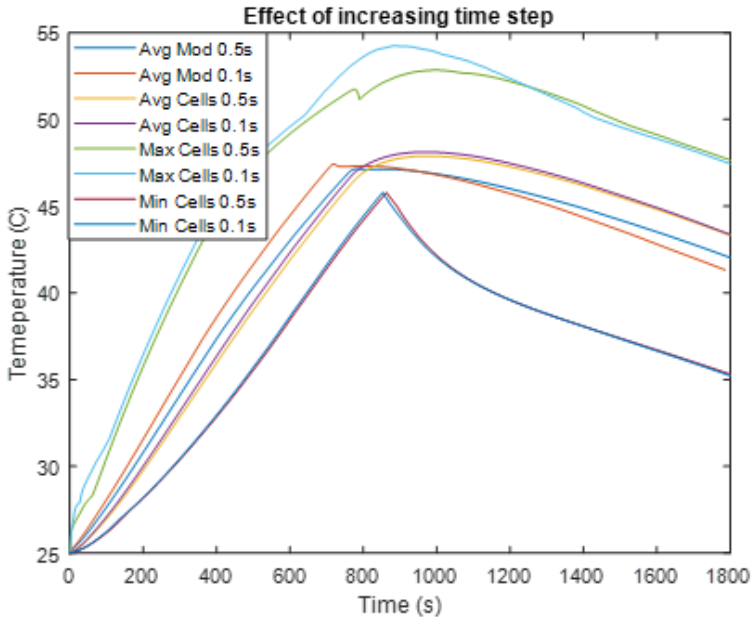

Figure 3.17: Effect of increasing timestep

4

Results

4.1 Sensitivity Analysis

To gain a clearer understanding of the system behaviour, several case studies are conducted focusing on two major parameters.

- Time step
- Entropic heat

4.1.1 Effect of increasing timestep

Considering reducing the computational cost, one strategy that is used is to increase the timestep from 0.1s to 0.5s, also discussed in the section: 3.11.1.2. Increasing the timestep potentially reduces the number of timesteps required for the simulation, decreasing computational time. However, it may also introduce approximations and affect the accuracy of the results. The purpose of this analysis was to achieve a good tradeoff between accuracy and computational cost. It is shown that even using a higher timestep i.e. 0.5s, doesn't have a significant effect on the results as shown in the figure 3.17.

4.1.2 Effect of Entropic Coefficient

The entropic coefficient data used for the cells is not the exact data from the supplier. Rather it's from another cell of similar chemistry [9]. The dependence of heat generation upon the entropic coefficient in the cell is also studied during fast charging. This will give an idea of the contribution of entropic heat to the total heat generation. For this purpose, first, the simulations are performed over a cell assuming no entropic heat generation. The results are then compared with the simulations performed with entropic heat generation as shown in figure 4.1. It can be seen from the results that when the entropic coefficient is smaller, then the heat generation with entropic changes is smaller and vice versa. It can be seen that the entropic heat has a slight contribution to the total heat. Thus, even using the data for a similar chemistry cell will not have a considerable effect on the results.

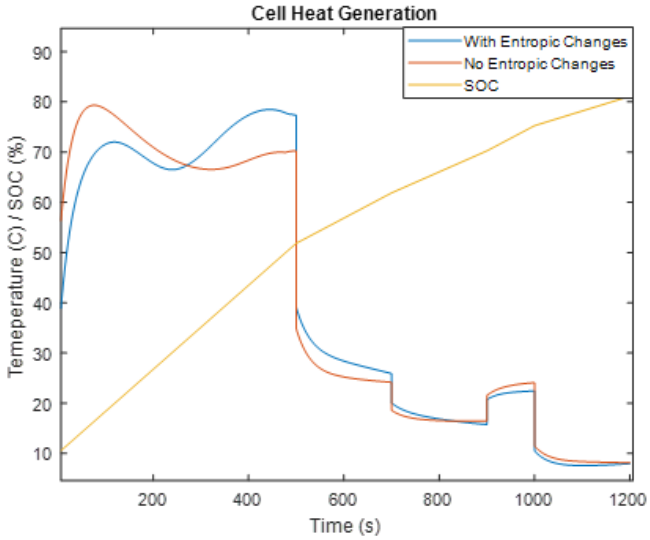

Figure 4.1: Variation of cell heat generation with entropic changes

4.2 Simulation Results

After developing the methodology, simulations were set up for a fast-charging event. For the module, the cell fast charging current in figure 3.12 is multiplied by three. This is because the cells are connected in 4s3p, as discussed in sec. 3.1. Using the conditions as shown in table 3.3, simulations are performed. Ensuring the convergence of the solution, the thermal behaviour of the module was studied. For this purpose, several variables like cell temperatures, temperature uniformity of cells and busbars temperatures were monitored during the complete fast charging event. Based on the module's thermal behaviour, as discussed below, the design was refined by making some adjustments, to have a more efficient thermal management system.

4.2.1 Identification of hotspots

The temperature contours are shown at the end of fast charging. It should be noted that it is not necessarily the time when the module is at peak temperature. However, the contours can still give an idea of the hotspots. The reason why identification of a hotspot is important is because this puts a limit on fast charging. If that is correctly pointed out, the design can be modified to distribute the temperature evenly in that area.

For design A (single plate cooling), the hotspots are in the top middle section of the cells over its length like figure 4.2. Therefore, it could be interesting to put another cooling plate over the top to conduct this heat too.

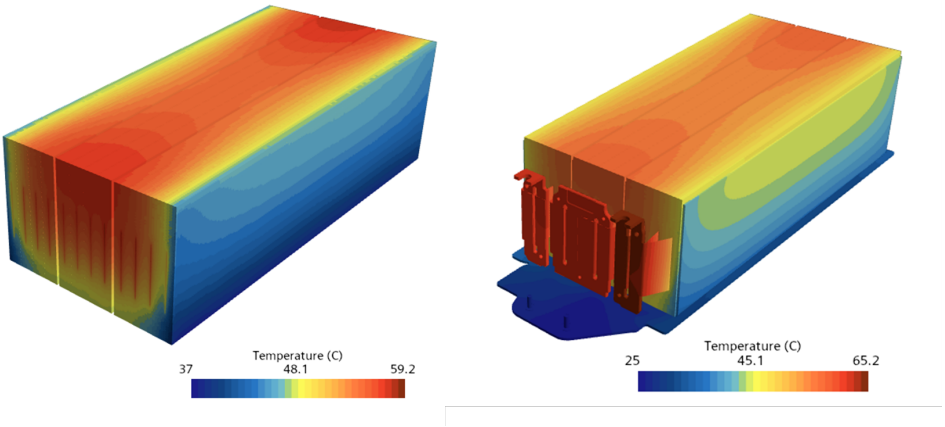

Figure 4.2: Temperature contours for Design A

In design B (Two plate cooling), since we have a cooling plate both on top and bottom, the temperature is more homogenous as seen in figure 4.3. But the area in the centre is still hot specifically on the two sides where we have busbar connections. If it has to be completely homogenized, a good idea is to place a heat pipe between the cells. The heat pipe will act as a faster way to transfer the heat to the cooling plate.

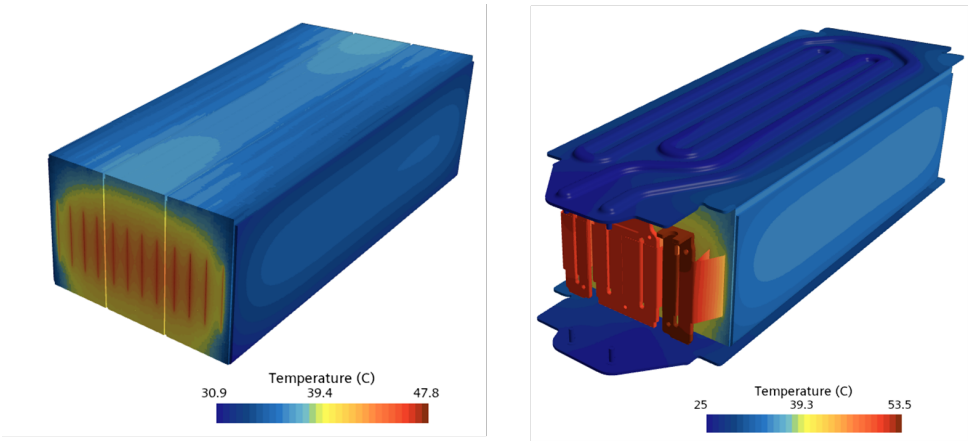

Figure 4.3: Temperature contours for Design B

For design C (Cooling plate with heat pipe), it can be seen that the temperature is almost the same to a very high degree. Looking closely at the contact between cells and cell tabs, there are some small, localized hotspots, figure 4.4. This is because of larger ohmic losses in the busbar/tab's region since they are not designed for such large currents.

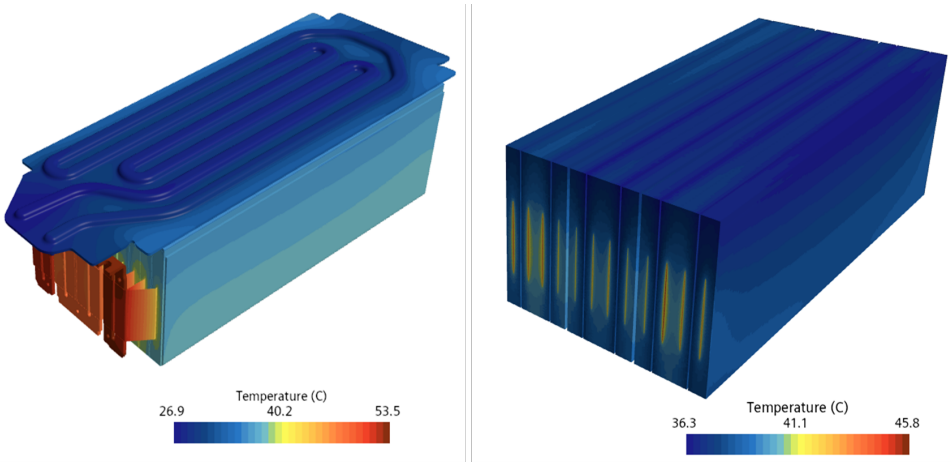

Figure 4.4: Temperature contours for Design C

4.2.2 Cell Temperature

One of the objectives of thermal management in a module is to keep the temperature of the cells in the optimum range. For this reason, the average, minimum and maximum temperature of the module are measured and monitored during the whole charging cycle. The maximum temperature in all the cases is the same (see figures 4.5 and 4.6) which is because the ohmic heat produced in the busbars but the maximum temperature is not a good measure to compare the designs because, in Design A, a large volume of cells can reach this temperature. However, for design C, it's a very small volume in the cell region. A good measure is the average temperature of the cells which is significantly lowered with design modification.

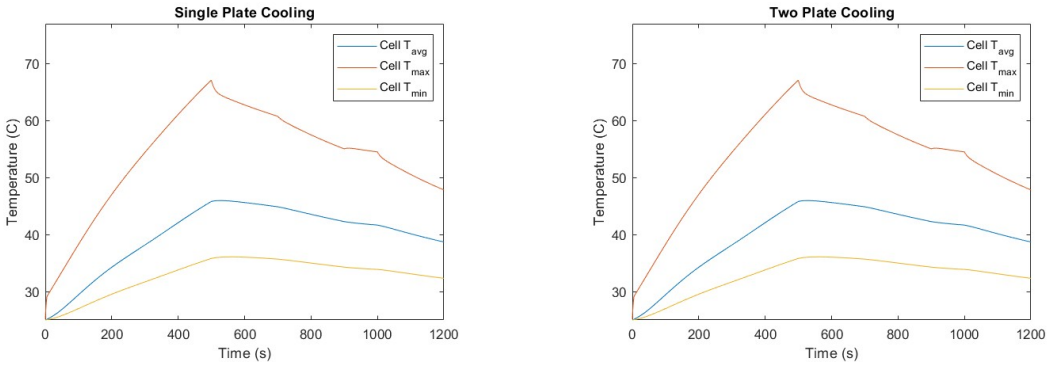

(a) Design A **(b)** Design B

Figure 4.5: Cell temperature

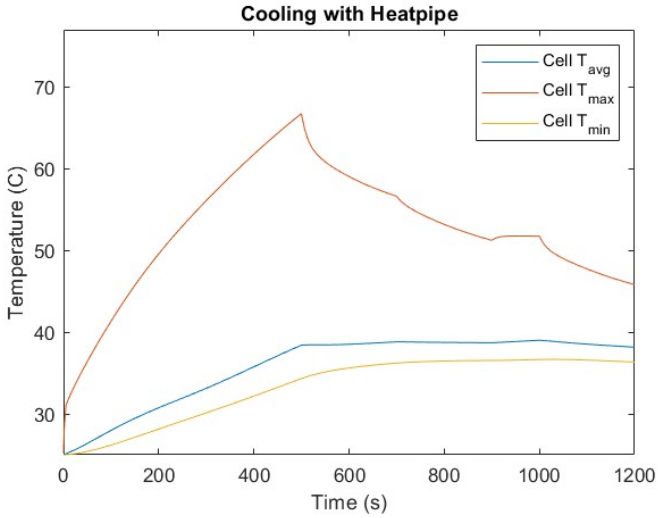

Figure 4.6: Cell temperatures for a single plate with heat pipe

4.2.3 Busbar/Tabs Temperature

The temperature in the busbar/tabs is significantly higher. This is not a huge problem since they are made of copper and aluminium. However, this higher temperature in this region is responsible for creating hotspots where they are connected with cells, see figures 4.7 and 4.8. It should be noted that the busbars and tabs are not meant for such high currents and in practice we don't see such higher temperatures.

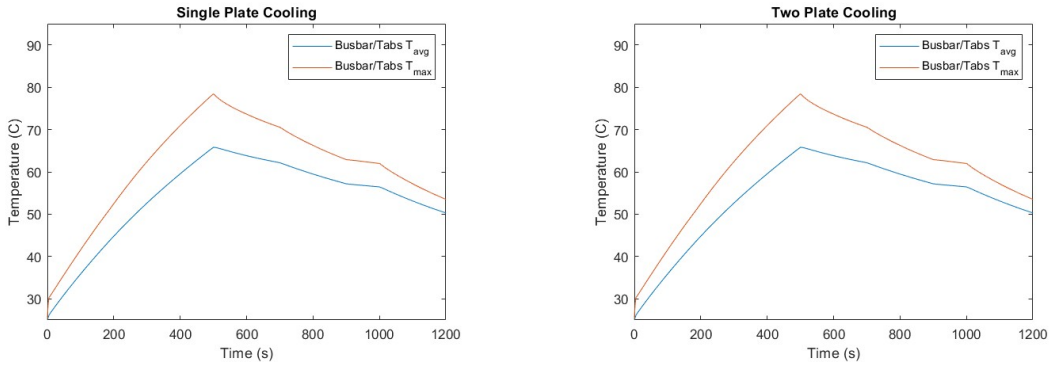

(a) Design A **(b)** Design B

Figure 4.7: Cells' temperature

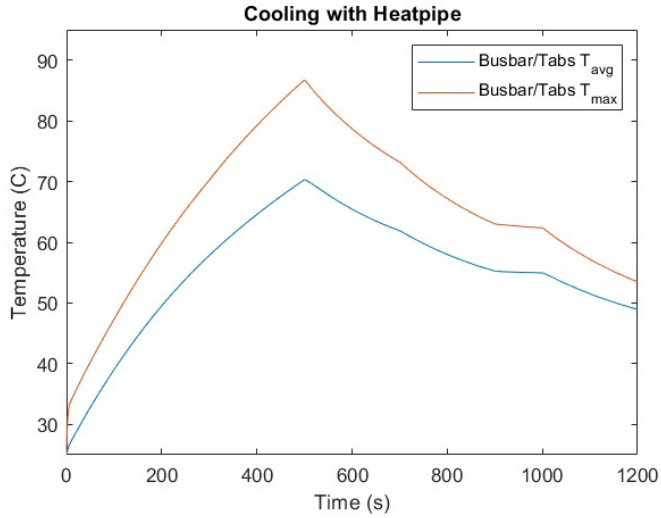

Figure 4.8: Busbar temperatures for a single plate with heat pipe

4.2.4 Temperature Uniformity

One of the main parameters for cells to have a longer life is having uniform temperature distribution in the cells. This is quantified by using the in-built field function in StarCCM+ "Standard Deviation". This shows how the temperature is scattered in the cell's region, figure 4.9. To have uniform temperature distribution, a lower standard deviation of temperature is desired with is achieved in Design C, figure 4.10. The higher values of standard deviation in temperature are not a problem in the busbar region because they are made of copper and their life won't be affected considerably by that.

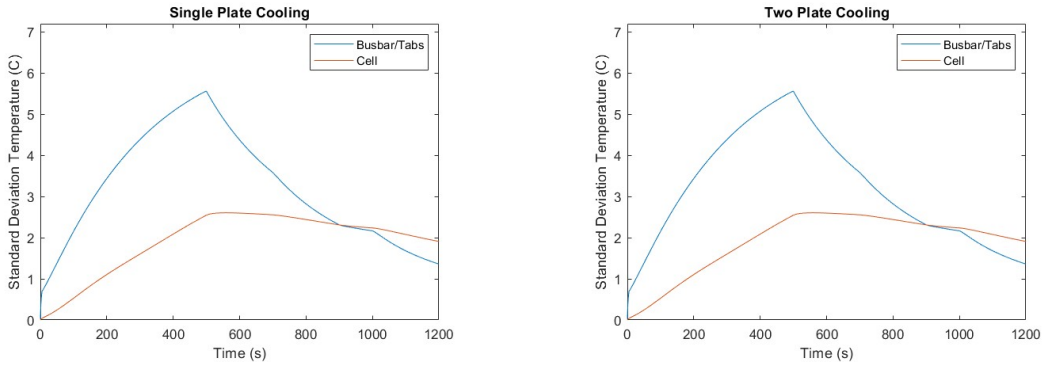

(a) Design A **(b)** Design B

Figure 4.9: Standard deviation for busbar

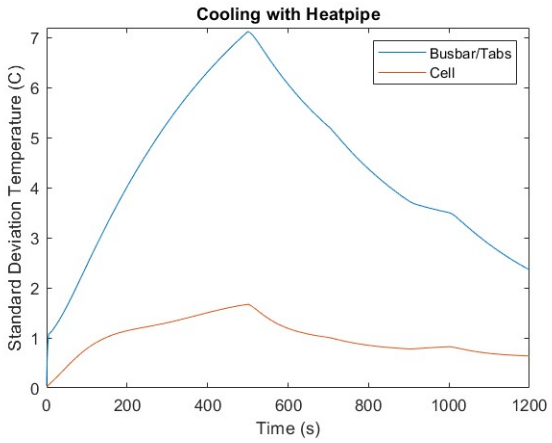

Figure 4.10: Standard deviation for a single plate with heat-pipe

4.3 Parametric study of heat-pipe

The heat pipe is a complex component that has fluid circulating across the two ends. The fluid also changes its phase during the heat transfer process. Simulating this phenomenon can be computationally expensive. In this method, the heat pipe was modelled such that its thermal conductivity is 10 times higher than copper. However, in reality, it won't be the case as there is a limit to the maximum heat transfer in the pipe. If it is required to extract more heat than is required, then the overall thermal conductivity of the pipe may decrease. To take this effect into account, a parametric study was conducted over the heat pipe by decreasing the value of thermal conductivity from around 4000 W/m-K to 1000 W/m-K in four steps. It can be seen from figure 4.11 that lowering the value of thermal conductivity increases the average temperature of the battery. A case is also studied when the heat pipe is replaced by just a copper plate. Considering the average temperatures of the cells, this design is better than just a single plate cooling but worse than the one with two plate cooling.

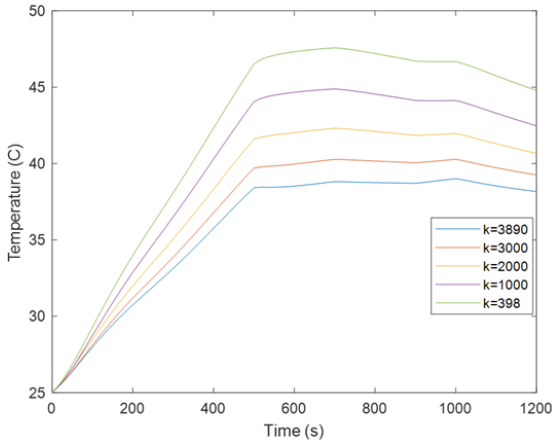

Figure 4.11: Parametric study of the heat-pipe

4.4 Verification from Experiments

Validating the model is an important step in any simulation. This involves comparing its predictions against the experimental data to determine the accuracy and reliability of the model. This will provide confidence in the accuracy of the CFD model and will allow for making informed decisions, optimizing design, and predicting its behaviour in different scenarios.

4.4.1 Test setup

A test is conducted at a fast-charging station on the vehicle (Polestar 2) that uses a battery module of the same geometry as shown in figure 3.2. The ambient conditions are not completely controlled as the test was conducted at a fast charging station shown in figure 4.12 . However, conducting the test in a lab environment could have produced more accurate results. The vehicle has sensors placed at different locations in the battery pack. By accessing the readings at the required sensors, the data was gathered to quantify the behaviour of the module during fast charging. This data was accessed by logging into the vehicle through a diagnostic tool. The limitation of this tool is that communication can be done with one sensor at a time. A delay of around 250-750ms was observed in the readings while accessing the software. This put a time limit on getting the next reading from the same sensor. However, this time difference was small enough to capture all the gradients. In this test, the initial SOC of the battery pack at 20% was increased to 80% in around 35 minutes.

Figure 4.12: Fast charge test

4.4.2 Test Results

During this test, data was collected from various sensors, including rotameters measuring coolant flow rates and thermocouples placed at strategic points such as the top surface of the middle cell, shown in figure 4.13, as well as at the coolant inlet and exit. Similarly, the current delivered by the charger and the corresponding SOC of the cell was also monitored. With the same conditions, results were also generated from the simulation model. Some of the collected data like coolant mass flow rate, current and inlet temperature was used as input for the simulation model. The temperature of the cells, at the same location where the sensor is placed in the vehicle, is tracked during fast charging in the simulation. The results for the temperature at the same location are shown in figure 4.14 to have a comparative analysis between the simulation results and experimental test.

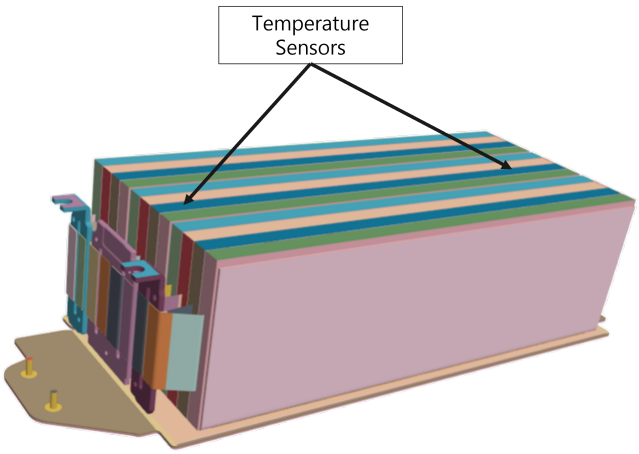

Figure 4.13: Location of temperature sensors

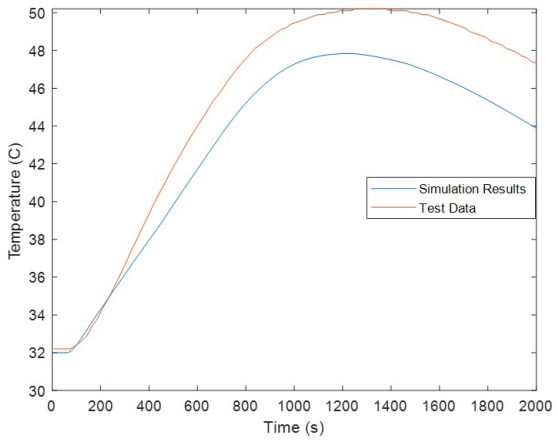

Figure 4.14: Comparison of simulation results against test data

4.4.3 Discussion of results

The analysis showed that the temperature trend at the same location is the same as the test results. However, there is a difference of a few degrees. This difference can be attributed to the limitations of the model. For example, the thermal properties of the cells e.g., Thermal conductivity and specific heat are not measured experimentally to accurately quantify cells' behaviour. In the model, a 0D ECM model was used to model the cells considering the cells' volume as a lumped mass. All the walls are assumed to be adiabatic, which was not the case during the experiment. It is also assumed that all the interfaces have a perfect contact except the contact between the frame and plate where it was assumed that the contact resistance between the frame and plate is 0.001 m2K/W. Ideally, all the contact resistances should be measured experimentally.

5
Conclusion

Managing the temperature of Li-ion batteries in an electric vehicle is crucial to ensuring safety and reducing battery degradation. This becomes more challenging during fast charging. Much higher currents flow throughout the battery cells that generate significant heat because of the ohmic losses. For this purpose, a methodology is developed to analyse the electro-thermal behaviour of a battery module. This method will enable the design of the battery module in such a way that the temperature stays in the optimum range even during fast charging. A good strategy for this method is to use a 0D ECM model to have a good trade-off between the model's complexity and accuracy. The proposed method explains how to setup up the model to perform a 3D CFD study for any condition. It was shown that the model can have good accuracy without incorporating entropic heat, however using the data for a similar chemistry is sufficient. The method is much more efficient in terms of computational cost as the different strategies e.g. freezing coolant flow, playing with time step, are implemented to bring down the simulation time from 28 hours to around 3 hours (if simulations are performed on a computer with 120 cores and 440GB RAM). The results of fast charging simulations show that a single plate cooling system is much more inefficient for the specific module. It was shown that the most effective approach is to implement a heat pipe between the cells to have a more uniform temperature distribution of the cells. The proposed method is also verified by conducting a fast-charging test experimentally and it was shown that the simulation results are in good agreement with the test results.

5.1 Limitations of the work

The cell is modelled using a 0D ECM that considers a cell as a lumped mass and assumes that the heat generation at a given instance is the same across the cell. However, in reality, temperature affects the resistance of the cell. As a result, more current will be flowing in the hotter region of the cell and hence more heat generation. A 0D model of a cell does not capture such details.

The contacts between different parts are assumed to be perfect. However, in reality, no contact is perfect as there will always be some gap. This will gap will act as a thermal barrier in the parts. However, to simplify this model, it was assumed that the thermal contact resistance of all the interfaces except the one between the cooling plate and frame is zero.

It is assumed that there is no heat transfer between the battery module and the ambient. This will only be the case when the module is at the same temperature as ambient.

The walls are assumed to be adiabatic and thus there is no heat transfer between the walls unless there is a contact between them. This will happen when it is in a vacuum. In practice, there will be air in the void spaces that will contribute to the heat transfer.

The heat pipe was modelled in such a way that it is like a copper plate but with a thermal conductivity of ten times that of copper. However, in reality, it has a fluid that is circulating inside. There is a limit to the amount of heat it can remove because of mass transfer limitations.

5.2 Future recommendations

Thermal runaway is a phenomenon that is observed above temperatures of $100°C$. It would be interesting if the thermal runaway is also modelled for the cell. By incorporating thermal runaway into this model, the temperature limits for this model can be expanded. This will enable to study the behaviour of the module can be studied at significantly higher temperatures.

A more accurate and quick model can be used for the heatpipe rather than just assigning a constant value of thermal conductivity. This will include modelling the thermal conductivity of the heat pipe as a function of the total heat transfer and the temperature differences experimentally.

It would be interesting to use a more accurate model to predict cell characteristics using the 3D ECM model. This can be done by designing the cell using “Battery Design Studio”, a software owned by SIEMENS. However, this can increase the computational cost.

Given that adiabatic conditions were assumed for all the walls, it would be beneficial to include the inclusion of air as a fluid in the empty spaces in the module. This will enable calculations of accurate heat transfer over the surface at a given condition.

The model can be accurately calibrated to the test data by playing around with different parameters like the cell thermal conductivity, cell-specific heat and thermal contact resistance.

5.3 Environmental and social impact of the work

This work has a significant environmental and social impact. Considering the environmental perspective, it helps in optimizing the energy efficiency of Li-ion batteries. As a result, the waste energy is reduced, and the overall performance is improved. A more efficient thermal management system will ensure the optimum temperature and reduce the higher temperature gradients in the cell. This will effectively increase their lifespan which is a more sustainable approach to the battery technology. In addition, the research increases battery safety by recognizing and managing thermal risks, lowering the possibility of accidents or fires, and avoiding environmental harm. This work increases battery performance, which benefits businesses that rely on Li-ion batteries specifically the ones involved in electromobility. Improved battery safety instils consumer trust, facilitating wider adoption of these technologies. This research contributes to the societal objective of reducing greenhouse gas emissions, improving air quality, and building a cleaner and healthier environment for communities through increasing sustainable mobility and encouraging energy efficiency.

This work targets the following 6 out of the 17 sustainable development goals set by United Nations [29].

1. **Affordable and Clean Energy:** Improving the Energy efficiency of Li-ion batteries through effective thermal management.

2. **Industry Innovation and Infrastructure:** Different innovative cooling solutions are explored.

3. **Sustainable cities and communities:** It indirectly supports this goal by improving the performance of Li-ion batteries and enabling the widespread adoption of electric vehicles.

4. **Responsible consumption and production:** Improving the lifespan of Li-ion batteries through innovative cooling strategies, supports this goal which encourages sustainable consumption and production patterns and improves resource efficiency.

5. **Climate Action:** Widespread adoption of electric vehicles enables us to reduce dependence on fossil fuels and combat climate change.

6. **Partnership for the goals:** The work can foster collaborations between academia and industry promoting knowledge and sharing technological advancements.

Figure 5.1: Relevant sustainable development goals by UN

Bibliography

[1] M. Broussely, P. Biensan, F. Bonhomme, *et al.*, "Main aging mechanisms in li ion batteries," *Journal of Power Sources*, vol. 146, no. 1–2, pp. 90–96, 2005. DOI: 10.1016/j.jpowsour.2005.03.172.

[2] D. Li, H. Li, D. Danilov, *et al.*, "Temperature-dependent cycling performance and ageing mechanisms of c6/lini1/3mn1/3co1/3o2 batteries," English, *Journal of Power Sources*, vol. 396, pp. 444–452, Aug. 2018, ISSN: 0378-7753. DOI: 10.1016/j.jpowsour.2018.06.035.

[3] X. Liu, W. Ai, M. Naylor Marlow, Y. Patel, and B. Wu, "The effect of cell-to-cell variations and thermal gradients on the performance and degradation of lithium-ion battery packs," *Applied Energy*, vol. 248, pp. 489–499, 2019. DOI: 10.1016/j.apenergy.2019.04.108.

[4] C. Arbizzani, G. Gabrielli, and M. Mastragostino, "Thermal stability and flammability of electrolytes for lithium-ion batteries," *Journal of Power Sources*, vol. 196, no. 10, pp. 4801–4805, 2011. DOI: 10.1016/j.jpowsour.2011.01.068.

[5] IEA, *Global ev outlook 2023 – analysis*. [Online]. Available: https://www.iea.org/reports/global-ev-outlook-2023.

[6] R. Casper and E. Sundin, "Electrification in the automotive industry: Effects in remanufacturing," *Journal of Remanufacturing*, vol. 11, no. 2, pp. 121–136, 2020. DOI: 10.1007/s13243-020-00094-8.

[7] J. S. Bartlett and B. Preston, *Automakers are adding electric vehicles to lineups*. [Online]. Available: https://www.consumerreports.org/cars/hybrids-evs/why-electric-cars-may-soon-flood-the-us-market-a9006292675/.

[8] C. Zhang, W. Allafi, Q. Dinh, P. Ascencio, and J. Marco, "Online estimation of battery equivalent circuit model parameters and state of charge using decoupled least squares technique," *Energy*, vol. 142, pp. 678–688, 2018. DOI: 10.1016/j.energy.2017.10.043.

[9] Z. Geng, J. Groot, and T. Thiringer, "A time- and cost-effective method for entropic coefficient determination of a large commercial battery cell," *IEEE Transactions on Transportation Electrification*, vol. 6, no. 1, pp. 257–266, 2020. DOI: 10.1109/tte.2020.2971454.

[10] M. Cheng, L. Sun, G. Buja, and L. Song, "Advanced electrical machines and machine-based systems for electric and hybrid vehicles," *Energies*, vol. 8, no. 9, pp. 9541–9564, 2015. DOI: 10.3390/en8099541.

[11] M. Cheng, L. Sun, G. Buja, and L. Song, "Advanced electrical machines and machine-based systems for electric and hybrid vehicles," *Energies*, vol. 8, pp. 9541–9564, Sep. 2015. DOI: 10.3390/en8099541.

[12] K. Murashko, J. Pyrhonen, and L. I. E. Laurila, "Three-dimensional thermal model of a lithium ion battery for hybrid mobile working machines: Determination of the model parameters in a pouch cell," *IEEE Transactions on Energy Conversion*, vol. 28, pp. 335–343, 2013.

[13] M. Zwicker, M. Moghadam, W. Zhang, and C. Nielsen, "Automotive battery pack manufacturing – a review of battery to tab joining," *Journal of Advanced Joining Processes*, vol. 1, p. 100 017, 2020. DOI: 10.1016/j.jajp.2020.100017.

[14] H. Löbberding, S. Wessel, C. Offermanns, *et al.*, "From cell to battery system in bevs: Analysis of system packing efficiency and cell types," *World Electric Vehicle Journal*, vol. 11, no. 4, p. 77, Dec. 2020, ISSN: 2032-6653. DOI: 10.3390/wevj11040077. [Online]. Available: http://dx.doi.org/10.3390/wevj11040077.

[15] R. Stadler and A. Maurer, "Methods for durability testing and lifetime estimation of thermal interface materials in batteries," *Batteries*, vol. 5, no. 1, p. 34, Mar. 2019, ISSN: 2313-0105. DOI: 10.3390/batteries5010034. [Online]. Available: http://dx.doi.org/10.3390/batteries5010034.

[16] J. Meng, M. Boukhnifer, D. Diallo, and T. Wang, "A new cascaded framework for lithium-ion battery state and parameter estimation," *Applied Sciences*, vol. 10, no. 3, p. 1009, 2020. DOI: 10.3390/app10031009.

[17] P. Jindal, R. Katiyar, and J. Bhattacharya, "Evaluation of accuracy for bernardi equation in estimating heat generation rate for continuous and pulse-discharge protocols in lfp and nmc based li-ion batteries," *Applied Thermal Engineering*, vol. 201, p. 117 794, 2022. DOI: 10.1016/j.applthermaleng.2021.117794.

[18] S. Chacko and Y. M. Chung, "Thermal modelling of li-ion polymer battery for electric vehicle drive cycles," *Journal of Power Sources*, vol. 213, pp. 296–303, 2012, ISSN: 0378-7753. DOI: https://doi.org/10.1016/j.jpowsour.2012.04.015. [Online]. Available: https://www.sciencedirect.com/science/article/pii/S037877531200746X.

[19] F. M. White and H. Xue, *Fluid mechanics*. McGraw Hill Education, 2021.

[20] K. Knoerzer, M. Regier, and H. Schubert, "A computational model for calculating temperature distributions in microwave food applications," *Innovative Food Science & Emerging Technologies*, vol. 9, no. 3, pp. 374–384, 2008. DOI: 10.1016/j.ifset.2007.10.007.

[21] S. Xin, C. Wang, and H. Xi, "Thermal management scheme and optimization of cylindrical lithium-ion battery pack based on air cooling and liquid cooling," *Applied Thermal Engineering*, vol. 224, p. 120 100, 2023, ISSN: 1359-4311. DOI: https://doi.org/10.1016/j.applthermaleng.2023.120100. [Online]. Available: https://www.sciencedirect.com/science/article/pii/S1359431123001291.

[22] S. Al-Hallaj and J. Selman, "Thermal modeling of secondary lithium batteries for electric vehicle/hybrid electric vehicle applications," *Journal of Power Sources*, vol. 110, no. 2, pp. 341–348, 2002, ISSN: 0378-7753. DOI: https:

//doi.org/10.1016/S0378-7753(02)00196-9. [Online]. Available: https://www.sciencedirect.com/science/article/pii/S0378775302001969.

[23] D. Kong, R. Peng, P. Ping, J. Du, G. Chen, and J. Wen, "A novel battery thermal management system coupling with pcm and optimized controllable liquid cooling for different ambient temperatures," *Energy Conversion and Management*, vol. 204, p. 112 280, 2020, ISSN: 0196-8904. DOI: https://doi.org/10.1016/j.enconman.2019.112280. [Online]. Available: https://www.sciencedirect.com/science/article/pii/S0196890419312865.

[24] M. Khan, H. A. Dhahad, S. Alamri, *et al.*, "Air cooled lithium-ion battery with cylindrical cell in phase change material filled cavity of different shapes," *Journal of Energy Storage*, vol. 50, p. 104 573, 2022, ISSN: 2352-152X. DOI: https://doi.org/10.1016/j.est.2022.104573. [Online]. Available: https://www.sciencedirect.com/science/article/pii/S2352152X22005904.

[25] A. Syrakos, O. Oxtoby, E. de Villiers, S. Varchanis, Y. Dimakopoulos, and J. Tsamopoulos, "A unification of least-squares and green–gauss gradients under a common projection-based gradient reconstruction framework," *Mathematics and Computers in Simulation*, vol. 205, pp. 108–141, 2023. DOI: 10.1016/j.matcom.2022.09.008.

[26] SIEMENS, *Star-ccm+ user guide*.

[27] A. Afzal, A. R. Kaladgi, R. Jilte, *et al.*, "Thermal modelling and characteristic evaluation of electric vehicle battery system," *Case Studies in Thermal Engineering*, vol. 26, p. 101 058, 2021. DOI: 10.1016/j.csite.2021.101058.

[28] [Online]. Available: https://support.sw.siemens.com/en-US/product/226870983/knowledge-base/KB000049946_EN_US..

[29] U. Nations, *The 17 sustainable development goals*. [Online]. Available: https://sdgs.un.org/goals.

A

Appendix 1

A.1 Temperature Contours

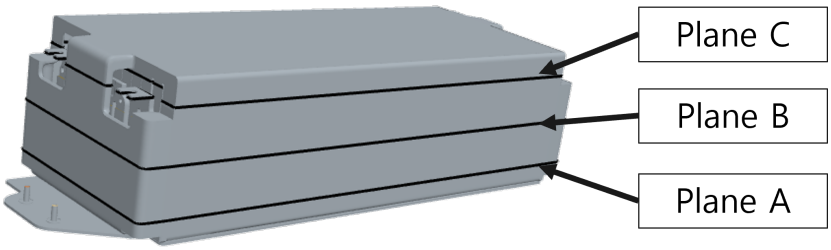

Figure A.1: Section Planes

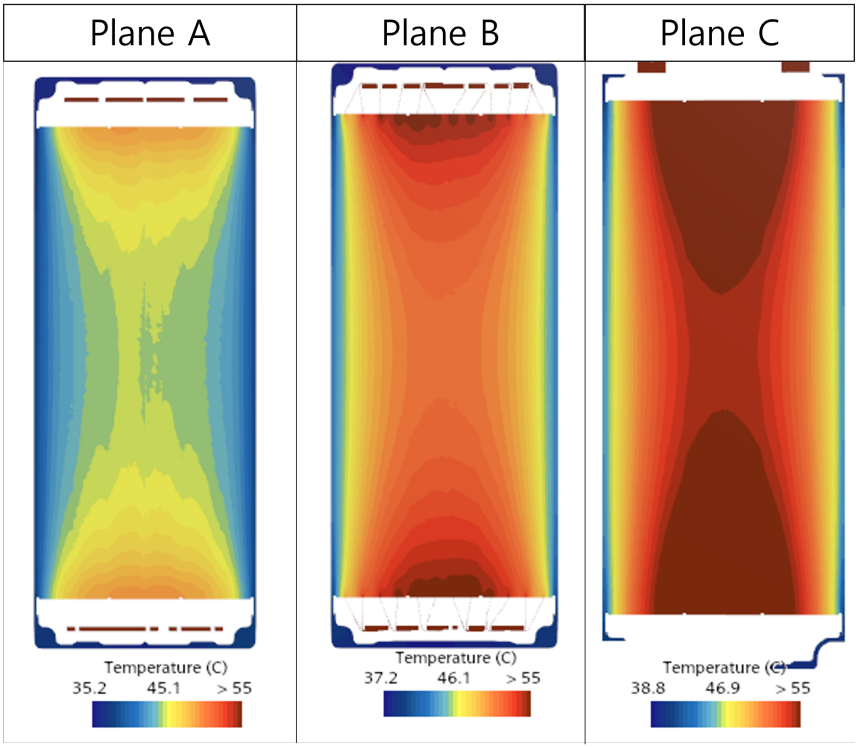

Figure A.2: Single Plate Cooling

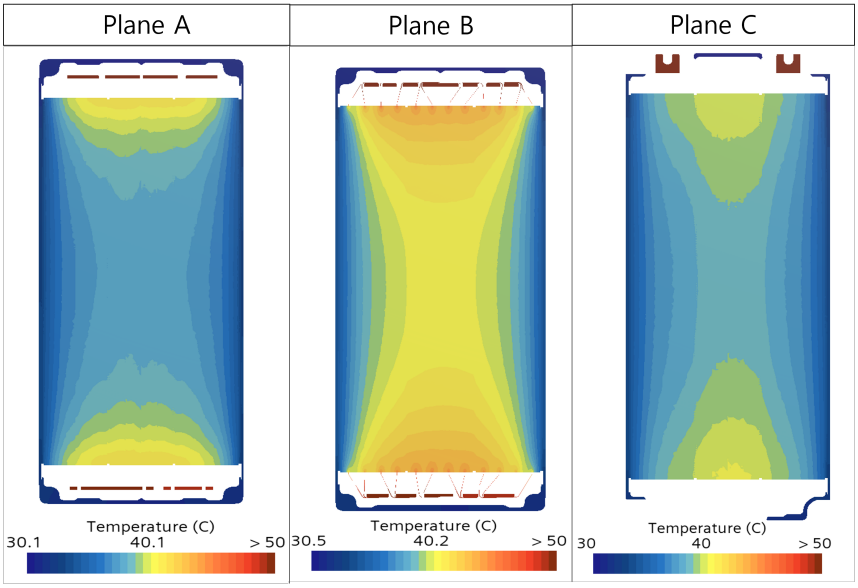

Figure A.3: Two Plates Cooling

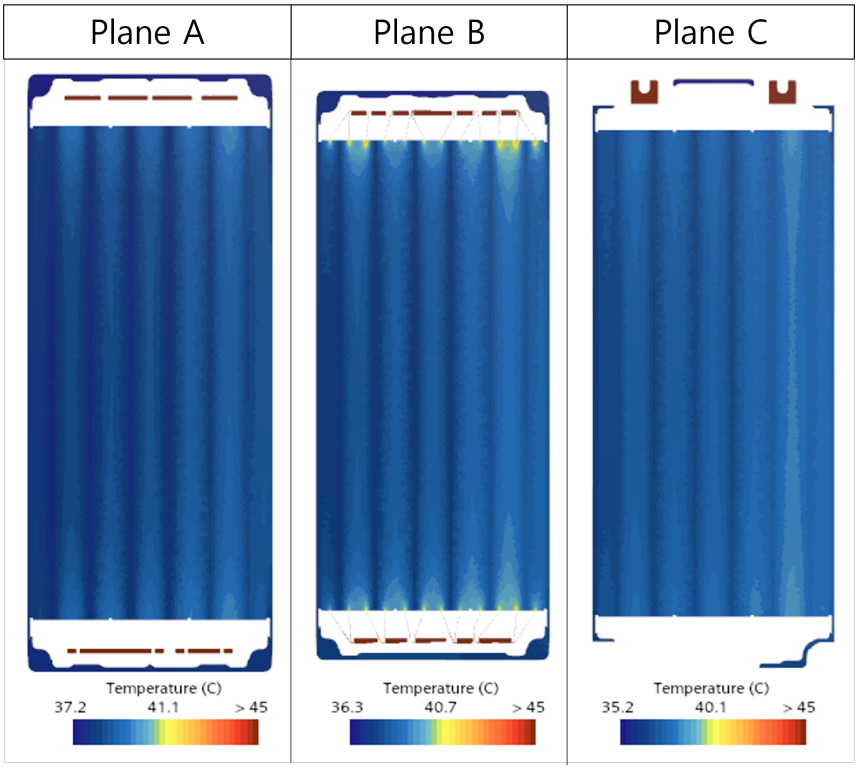

Figure A.4: Cooling with Heatpipe

A.2 Mesh Quality Check

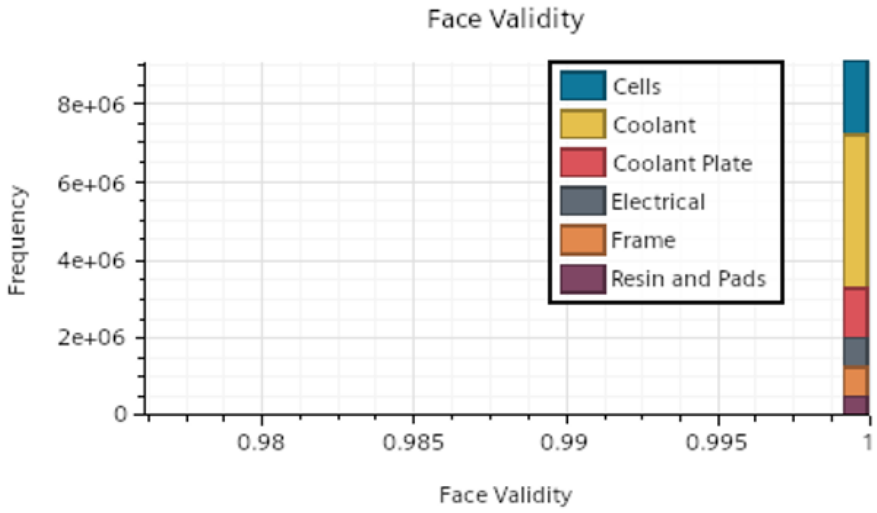

Figure A.5: Face Validity

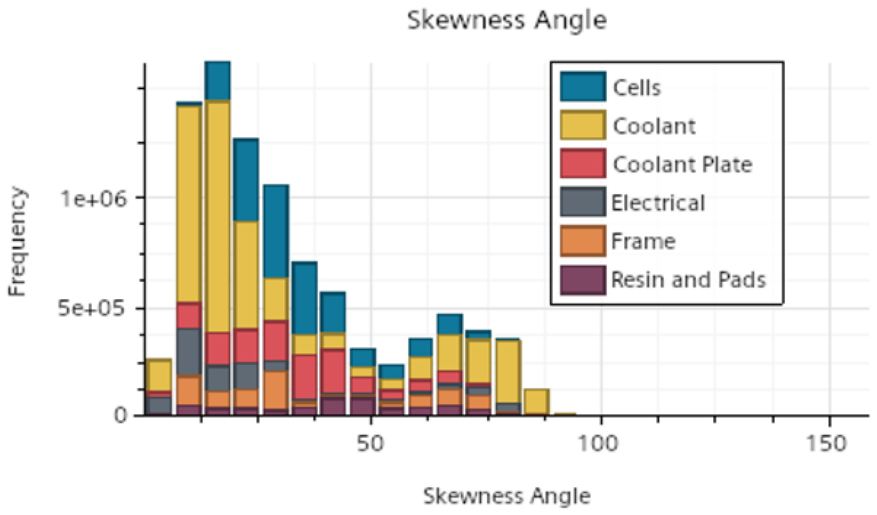

Figure A.6: Skewness Angle

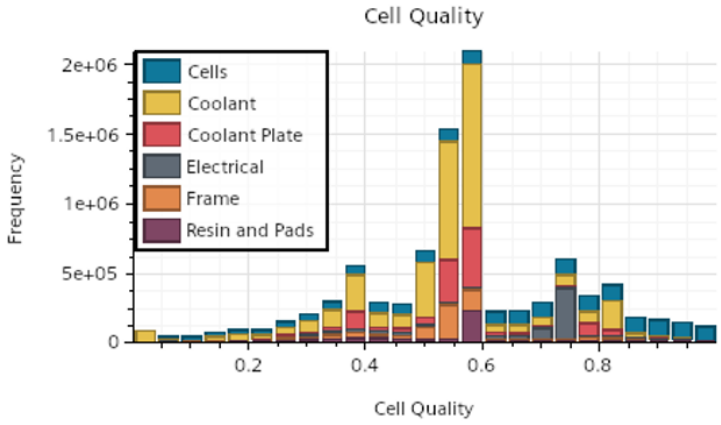

Figure A.7: Cell Quality

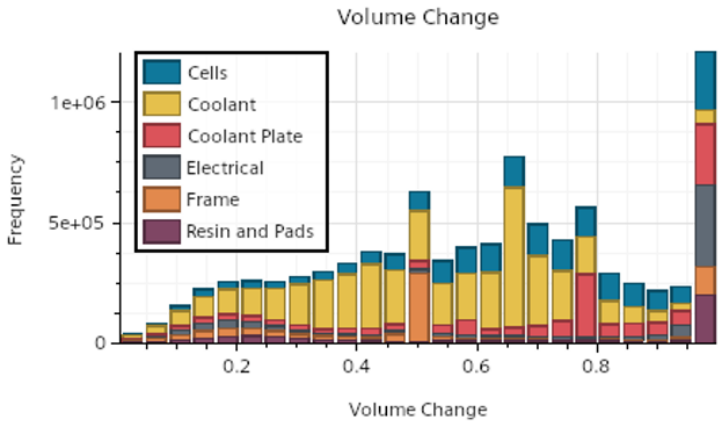

Figure A.8: Volume Change

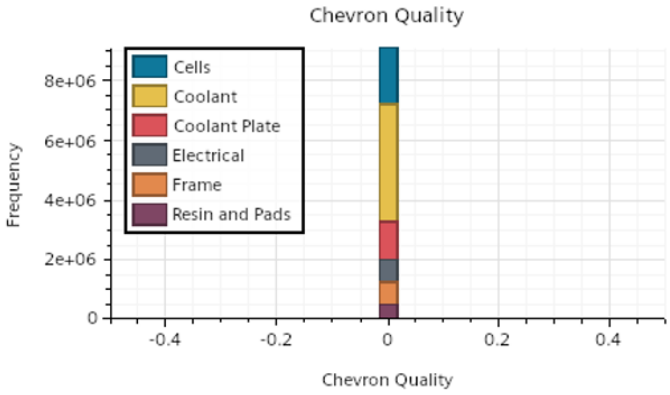

Figure A.9: Chevron Quality

A.3 Fast Charging Test

Figure A.10: Jens logging data from the car using the diagnostic tool

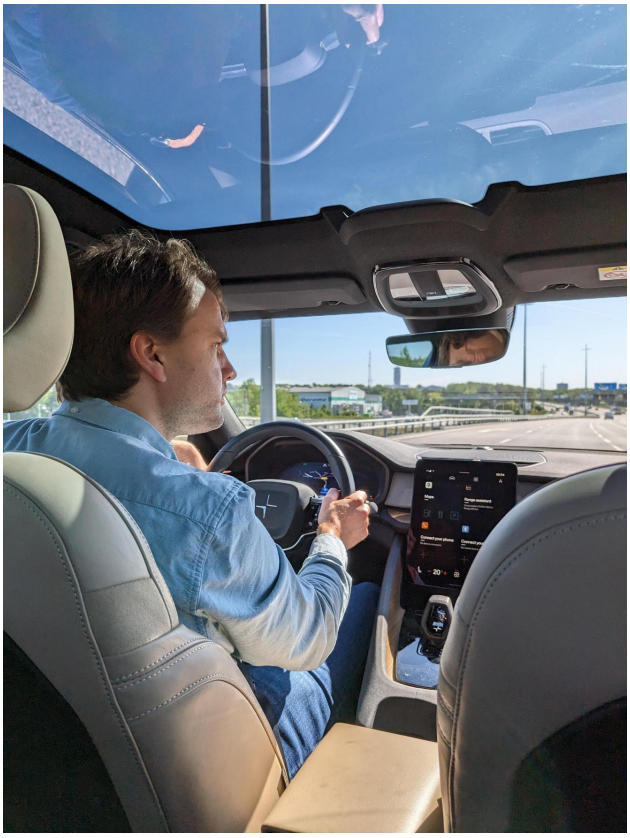

Figure A.11: Anders driving us to the charging station

A.4 Optimization of Charging Curve

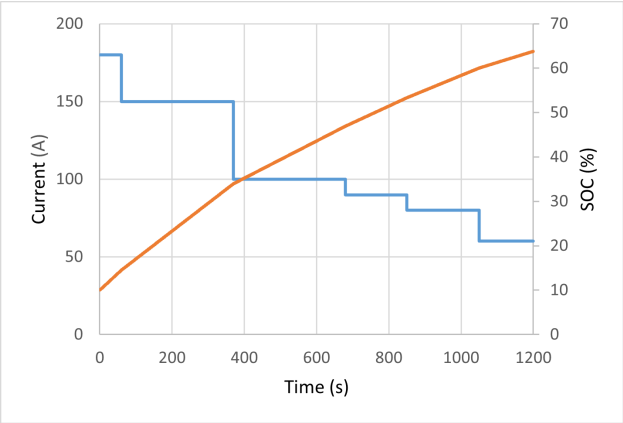

Figure A.12: First Iteration

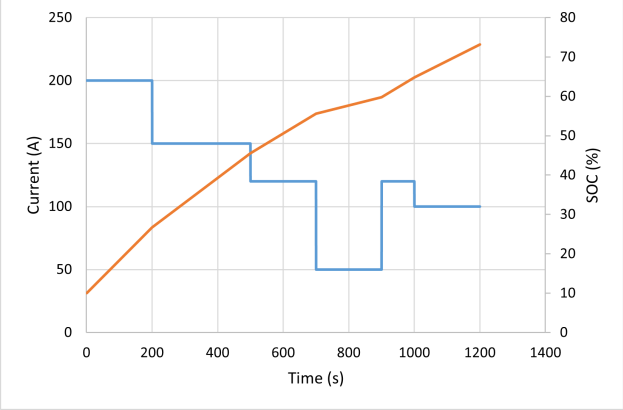

Figure A.13: 2nd Iteration

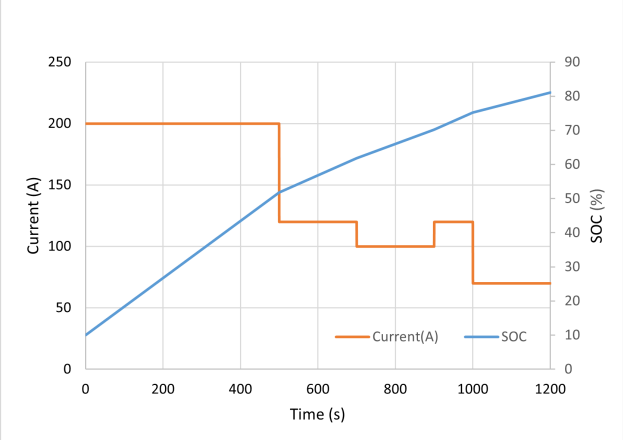

Figure A.14: Optimized Charging Curve

A.5 Code for ECM parameter fitting

```
close all;
clear all;

%% Experimental Data
Data=readmatrix("25C_Discharge.xlsx");       % DC-IR data
% First Col. SOC, Next is IR value at 1s, 2s, 5s, 10s, 18
   s, 30s
OCV_data=readmatrix("OCV_Discharge.xlsx");  % OCV Data
% First Col SOC, Next temp -10C, 10C, 25C, 45C

%% Test Specifications
Cap=66;                     % Battery capacity in Ah
C_rate=5;                   % Discharge Rate
Current=C_rate*Cap;         % Discharge Current
Pulse_time=30/3600;         % Time in hours


SOC_Change=-Pulse_time*100*C_rate;

Counter=1;
Results=zeros(9,5);
for SOC_init=90:-10:0
    Counter=Counter+1;
    SOC_init;
    IR=Data(Counter,2:7);
    ts = [1 2 5 10 18 30]/3600;
    SOC=SOC_init-(ts*100*C_rate);

    % Correcting OCV for SOC Change
    OCV_fun=@(x) interp1(OCV_data(:,1)./100,OCV_data(:,4)
       ,x/100);
    OCV=OCV_fun(SOC);
    dOCV=zeros(1,6);
    for i=1:5
        dOCV(i+1)=OCV(i)-OCV(i+1);
    end
    if SOC_init==0
        dOCV(:)=0;
    end

    time = [1 2 5 10 18 30];
    Rs = IR/1000;
    Us = Rs * Current;

```

```
43      % First estimating R0 by linear extrapolation from 1s
            and 2s values
44      R0 = 2*Rs(1) - Rs(2);
45      C1=30;
46
47      % Defining a function to fit R1; R1*C1 is fixed at 30
            s as the available data
48      % cannot easily give robust values for R1 and C1
49      f = @(x,t)  Current* R0 + Current * x(1) * (1 - exp(-
           t/(C1)));
50
51      p_opt = lsqcurvefit(f,[1/500],time,Us-dOCV);
52
53      %Results
54      Results(Counter-1,:)=[SOC_init OCV_fun(SOC_init) R0
           p_opt C1];
55
56  end
```

DEPARTMENT OF MECHANICS AND MARITIME SCIENCES
CHALMERS UNIVERSITY OF TECHNOLOGY
Gothenburg, Sweden
www.chalmers.se

CHALMERS
UNIVERSITY OF TECHNOLOGY